Postseismic gravity changes observed from GRACE satellites:
The two components of postseismic gravity changes and their mechanisms

重力衛星 GRACE を用いた地震後重力変化の研究：
余効変動の二成分の分離とそのメカニズムの考察

Space Geodesy, Earth and Planetary Dynamics
Department of Natural History Sciences,
Graduate School of Science, Hokkaido University

Yusaku Tanaka

Supervisor: Prof. Kosuke Heki

北海道大学 大学院 理学院 自然史科学専攻
地球惑星ダイナミクス講座 宇宙測地学研究室

田中 優作

指導教官：日置 幸介 教授

February 2014

ABSTRACT

The time series analysis of the gravity changes of the three M_w9-class mega-thrust earthquakes, i.e. the 2004 Sumatra-Andaman earthquake, the 2010 Chile (Maule) earthquake, and the 2011 Tohoku-oki earthquake, provides the possibility to identify their multiple postseismic phenomena. We have three sensors for earthquakes. The first sensor is seismometers, and we can measure seismic waves with them. The second sensor, such as GNSS (Global Navigation Satellite System) and SAR (Synthetic Aperture Rader), can measure crustal movements associated with earthquakes. The third sensor is gravimetry. The first sensor cannot catch the signal of postseismic phenomena because they do not shake the ground. The second sensor can catch the signal of postseismic phenomena, but they cannot separate phenomena, such as afterslip and viscous relaxation, because these mechanisms let the ground move in the same polarity. However, these postseismic processes may result in different polarities in gravity changes. This suggests that the gravity can be a powerful sensor to separated signals of different postseismic processes.

GRACE (Gravity Recovery And Climate Experiment) is the twin satellite systems launched in 2002 by NASA (National Aeronautics and Space Administration) and DLR (German Space Agency). It provides the two-dimensional gravity field of the earth with high temporal and spatial resolution. GRACE gives us insights into mass movements beneath the surface associated with earthquakes. The gravity time series before and after large earthquakes with GRACE suggest that the gravity (1) decreases coseismically, (2) keeps on decreasing for a few months, and (3) increases over a longer period. In other words, the postseismic gravity changes seem to have two components, i.e. the short-term and the long-term components. This new discovery suggests that the gravity observations detected two different postseismic processes with opposite polarities.

The mechanisms of coseismic gravity changes are relatively well known but those of short- and long-term postseismic gravity changes are not so clear at the moment. They are explained with afterslip and viscoelastic relaxation to some extent, but problems still remain. Nevertheless, the gravity observation can do what seismometers and GNSS/SAR cannot do, i.e. to separate different postseismic processes giving rise to gravity changes in different polarities.

概要

本研究では，重力衛星 GRACE (Gravity Recovery And Climate Experiment) が捉えた超巨大逆断層型地震（2004 年スマトラーアンダマン地震，2010 年チリ（マウレ）地震，2011 年東北沖地震）に伴う重力変化を時系列解析することで，重力が地震後に地球内部で起こっている現象を分離して観測できる第一の手段になりうることを示した．地震を観測するセンサーは今のところ三種類ある．第一のセンサーは地震計であり，第二のセンサーは GPS (Global Positioning System) を始めとする GNSS (Global Navigation Satellite System)及び SAR (Synthetic Aperture Rader)などの宇宙技術を用いた地殻変動の観測手法，そして重力観測が第三のセンサーである．地震計は地震波を捉え，GNSS や SAR は地殻変動を空から観測し，重力は質量移動を追跡する．地震「時」の現象はどのセンサーでも捉えることができる．しかし地震「後」の現象は，地震波を出さないため地震計では捉えられない．地震後の地表の動きは GNSS や SAR が捉えることができる．しかし，それらも地下で複数のメカニズム（余効すべりや粘弾性緩和）による過程が起こっていた場合，それらを分離して捉えることは難しい．可能なのは，いくつかの仮定を置いた上で，複数の現象に対応したモデル計算を行い，その結果と観測結果の一致を得ることである．しかし，地震後に複数のメカニズムで変動が起こっている場合，もっと望ましいのは，そのメカニズムの各々を別々に観測値として得ることだろう．本研究で発見したのは，地震後に起こる変動が重力としては、逆の極性でかつ異なる時間スケールで観測されることである．これは重力が地震後に地球内部で起こっている現象を区別して観測できる第一の手段である可能性を強く示している．

CONTENTS

1 Introduction

1.1 Space Geodesy in geoscience

Space geodesy is the discipline of the shape, size, gravity fields, rotation, and so on, of the earth, other planets, and the moon with space techniques. Geodesy with satellite started in 1957, when the first satellite "Sputnik I" was launched by the Soviet Union. Space geodesy has been applied to many disciplines in geoscience, and has contributed to their advances. For example, GPS (Global Positioning System) and SAR (Synthetic Aperture Radar) are applied to seismology, volcanology, meteorology, solar terrestrial physics, and so on. This is because observations from satellites are often superior to those on the ground in various aspects. One is the temporal continuity: satellites keep providing observation data until they stop functioning. Another aspect is that huge amount of data will eventually become available to researchers, giving all scientists chances to study using such data. One more aspect is that satellites often give two-dimensional observation data with uniform quality. This cannot be achieved by deploying many sensors on the ground. These aspects make space geodesy a very important approach in geosciences.

1.2 Satellite gravimetry

Gravity measurements in general have played and will continue to play important roles in earth sciences because they provide much information on the matters beneath the surface that we cannot see directly; the gravity fields reflect how mass is distributed there.

Satellite gravimetry started in 1958, when USA launched the satellite "Vanguard I". Tracking of this satellite enabled us to estimate low degree/order gravity field of the earth for the first time. Satellite gravimetry can be done in several different ways. The first one is SLR (Satellite Laser Ranging), which started in late 1960s. Satellites for SLR have a lot of corner-cube-reflectors (CCR) on their surfaces. The CCRs reflect laser pulses emitted from the ground station, and people can measure the two-way travel times of the laser pulses between the ground station and the satellites. The changes in orbital elements depend on the gravity, so we can recover the gravity field model. SLR has some benefits. First of all, it is relatively easy to continue the operation of SLR satellites because they have only passive function to reflect laser pulses with CCRs (they do not need batteries). Another benefit is that SLR is a relatively old technique, and we can go back further in time.

The second type is composed of "twin" satellites, and is represented by GRACE (Gravity Recovery And Climate Experiment), launched in 2002. The gravity irregularities change not only the orbital parameters of satellites but also their velocities. Then, the relative velocity between the two satellites tells us how different the gravity fields are between the two satellites.

GRACE has good spatial and temporal resolution. The spatial resolution of GRACE is 300~500 km. This is much better than that of SLR because the GRACE orbit is much lower than SLR satellites. For example, LAGEOS, one of the most useful SLR satellites, has an orbit as high as about 6000 km. The temporal resolution of GRACE is about one month, which is better than GOCE (Gravity field and steady-state Ocean Circulation Explorer), the third type of satellites to measure the gravity field with an on-board gradiometer. GOCE is called "Ferrari of the satellites" because it flies the lowest orbit of the satellites (this means its speed is the highest). GOCE has the best spatial resolution of the three types. Each type of satellites has its benefit and has produced valuable sets of data.

1.3 Gravity and earthquakes

Gravity observation is considered to be the third approach to understand earthquakes. The first sensor is seismometers to observe elastic (seismic) waves, and the second sensor is GNSS (Global Navigation Satellite System) like GPS and SAR to observe static displacement of the ground surface. Gravimetry, the third sensor, can observe the mass transportation under the ground.

There are two kinds of gravity changes due to earthquakes: co- and postseismic gravity changes (we do not discuss preseismic changes here). The mechanisms responsible for coseismic gravity changes have been understood to a certain extent. The coseismic gravity change occurs in two processes, i.e. (1) vertical movements of the boundaries with density contrast, such as the surface and Moho, and (2) density changes in mantle and crust. They are further separated into four: surface uplift/subsidence, Moho uplift/subsidence, dilatation and compression within crust and mantle. For submarine earthquakes, movement of sea water also plays a secondary role. These mechanisms are shown in Figure 1.1. The mechanisms of postseismic gravity changes are, however, not so clear.

Coseismic gravity change was first detected after the 2003 Tokachi-oki earthquake (M_w8.0), Japan, by a ground array of superconducting gravimeters [*Imanishi et al.*, 2004]. The second example (also the 1st example with satellite gravimetry) was coseismic gravity changes by the 2004 Sumatra-Andaman earthquake (M_w9.2) detected by the GRACE satellites [*Han et al.*, 2006]. Satellite gravimetry enabled similar studies for the 2010 Maule (M_w8.8) [*Heki and Matsuo*, 2010; *Han et al.*, 2010] and the 2011 Tohoku-Oki (M_w9.0) [*Matsuo and Heki*, 2011; *Wang et al.*, 2012] earthquakes. These reports showed that coseismic gravity changes are dominated by the decrease on the back arc side of the ruptured fault reflecting the density drop of rocks there [*Han et al.*, 2006].

Postseismic gravity changes were first found for the 2004 Sumatra-Andaman earthquake [*Ogawa and Heki*, 2007; *Chen et al.*, 2007]. They showed that the gravity increased after coseismic decreasing (Figure1.2) by fitting the function (1.1) with the least-squares method. They also revealed that postseismic gravity changes show opposite polarity and slight trenchward shift, i.e. gravity increase occurred directly above the ruptured fault.

For the other two M_w9-class earthquakes (2010 Maule and 2011 Tohoku), the time series of postseismic gravity changes have not been reported yet. Here we use the newly released Level-2 (RL05) GRACE data, which were improved in accuracy [*Dahle et al.*, 2012; *Chambers and Bonin*, 2012], and study common features in the co- and postseismic gravity changes of these megathrust earthquakes.

I model the gravity G as a function of time t as follows,

$$G = a + bt + c\,sin(\omega t + \theta_1) + d\,sin(2\omega t + \theta_2) + H(t)\left\{\Delta g + e\left(1 - \exp\left(\frac{\Delta t}{\tau}\right)\right)\right\} \quad (1.1)$$

$$H(t) = \begin{cases} 0 \; (t < t_0) \\ 1 \; (t \geq t_0) \end{cases}$$

$$\Delta t = t - t_0$$

where *a, b, c, d,* and *e* are the constants to be estimated with the least-squares method, t_0 is the time when the earthquake occurred, the second term means the secular trend, the third and fourth terms correspond to the seasonal changes ($\omega \equiv 2\pi/1\text{yr}$), Δg is the coseismic gravity step, and the last term is the postseismic gravity change. $H(t)$ is the step function, and τ is the time constant.

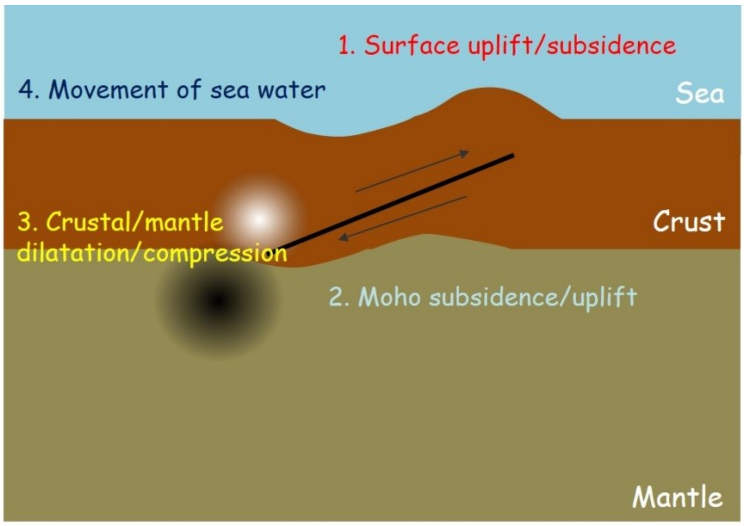

Figure 1.1 The four major mechanisms responsible for coseismic gravity changes.

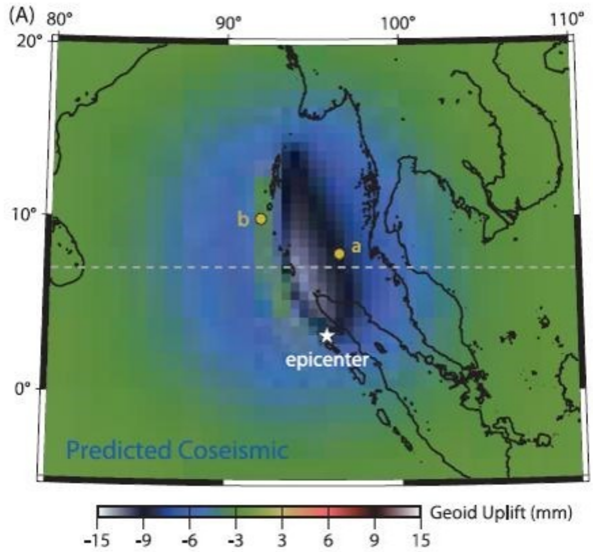

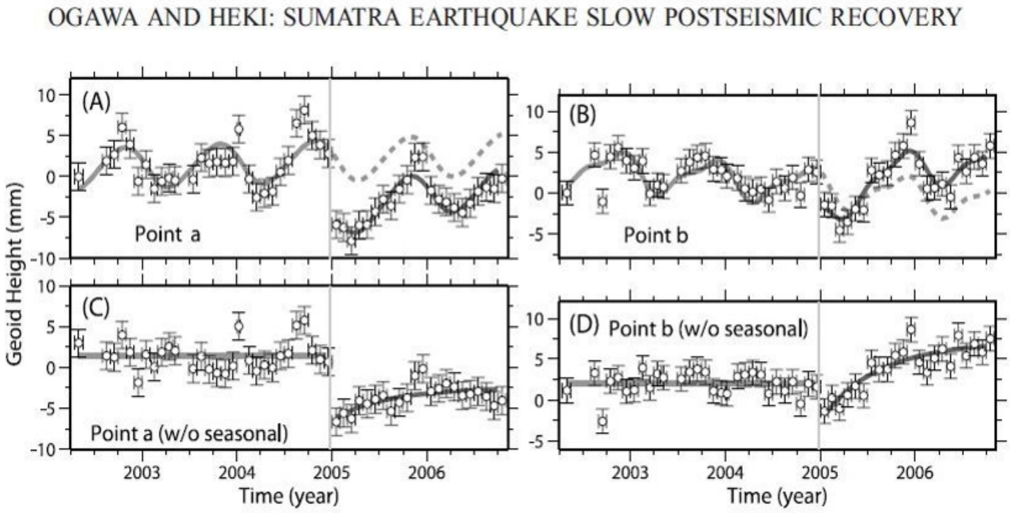

Figure 1.2 The postseismic geoid height changes of the 2004 Sumatra-Andaman earthquake shown by *Ogawa and Heki* [2007]. The geoid height decreased when the earthquake occurred and increased slowly afterwards.

2 Data and Methods

2.1 GRACE data

GRACE data can be downloaded from http://podaac.jpl.nasa.gov/ (PO.DAAC: Physical Oceanography Distributed Active Archive Center) or http://isdc.gfz-potsdam.de/ (ISDC:

Information Systems and Data Center). These data are provided by the three research centers, i.e. UTCSR (University of Texas, Center for Space Research), JPL (Jet Propulsion Laboratory), and GFZ (GeoForschungsZentrum, Potsdam). UTCSR and JPL are in USA, and GFZ is in Germany. These three institutions analyze data based on somewhat different approaches so the data sets differ slightly from center to center.

There are three levels of GRACE data available to the users: Level-1B, Level-2, and Level-3. Level-1B gives the data of the ranges (distances) between the twin satellites together with their changing rates, and it takes some expertise in technical details to use them. Level-2 data are provided as spherical harmonic coefficients, and we need only certain mathematical knowledge to use them. Level-3 data are composed of space domain gravity data after being filtered in several ways. Because it takes neither technical nor mathematical knowledge to use them, Level-3 is the most friendly to users. However, Level-3 data do not give us much information because many filters have already been applied. In this study, Level-2 data analyzed at UTCSR are used.

Level-2 data are composed of spherical harmonic coefficients (Stokes' coefficients). They coefficients can be converted to the static gravity field g (θ, ϕ) of the earth by the equation (2.1) [*Kaula*, 1966; *Heiskanen and Moritz*, 1967].

$$g(\theta, \varphi) = \frac{GM}{R^2} \sum_{n=2}^{nmax} (n-1) \sum_{m=0}^{n} (C_{nm} \cos m\varphi + S_{nm} \sin m\varphi) \overline{P_{nm}}(\sin \theta) \qquad (2.1)$$

Where G is the universal gravity constant, M is the mass of the earth, R is the equatorial radius, $P_{nm}(\sin \theta)$ is the n-th degree and m-th order fully-normalized associated Legendre function. An example of the static gravity field of the earth is shown in the Figure 2.1.

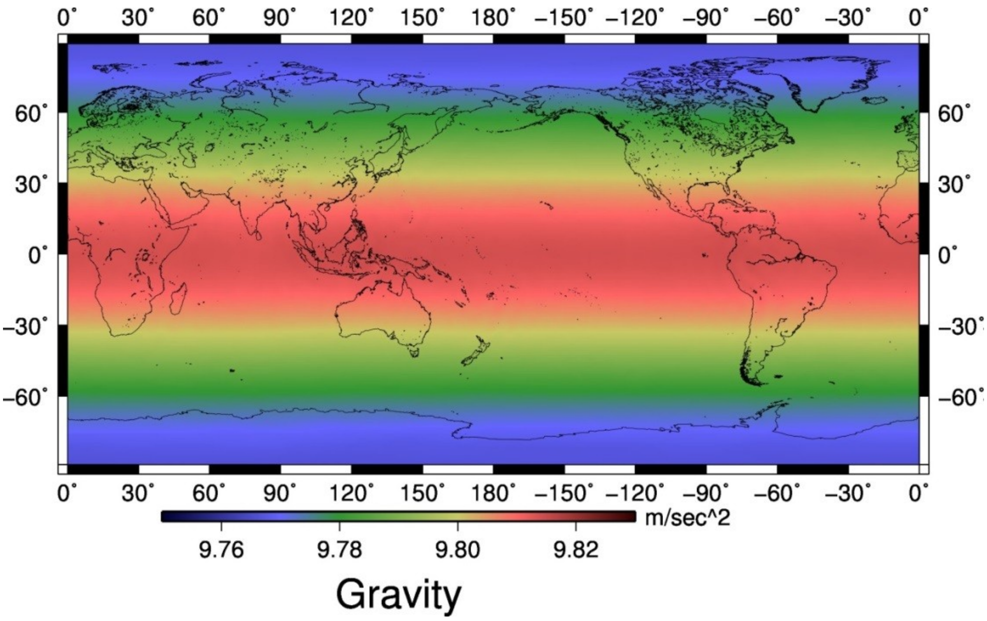

Figure 2.1 The map of the static gravity field of the earth in November 2013 calculated from Level-2 GRACE data. Degrees and orders of spherical harmonic coefficients are up to 60.

Figure 2.1 shows the mean of the gravity is about 9.8 m/s^2 and the gravity on lower latitude is stronger than that on higher. But this is contradictory to the fact that the gravity on lower latitude is weaker because the centrifugal force of the rotation of the earth works. The reason of this contradiction is that the gravity fields measured by satellites do not include centrifugal forces and gravitational pull of the equatorial bulge is isolated. Because the C_{20} term predominates in the earth's gravity fields, I removed it and plot the rest of the gravity components in Figure 2.2. When we discuss time-variable gravity, we use C_{20} from SLR observations because C_{20} values by GRACE are less accurate.

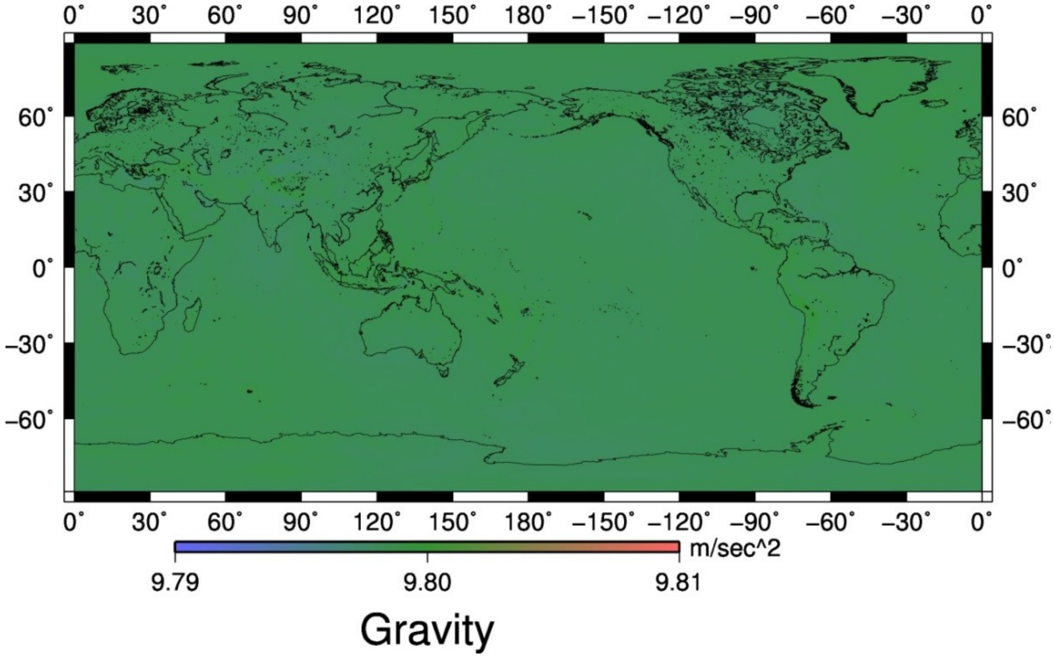

Figure 2.2 The map of the static gravity field of the earth in November 2013 calculated from Level-2 GRACE data after removing the C_{20} component.

Figure 2.2 shows that the gravity anomaly is so small that gravity is uniformly 9.8 m/s^2 throughout the surface. In order to highlight the gravity anomalies, we should use the unit of mGal (1Gal = 1cm/s^2) and should also make C_{00} zero because it gives the mean value of the gravity field. Figure 2.3 and Figure 2.4 show the gravity anomaly with the unit mGal.

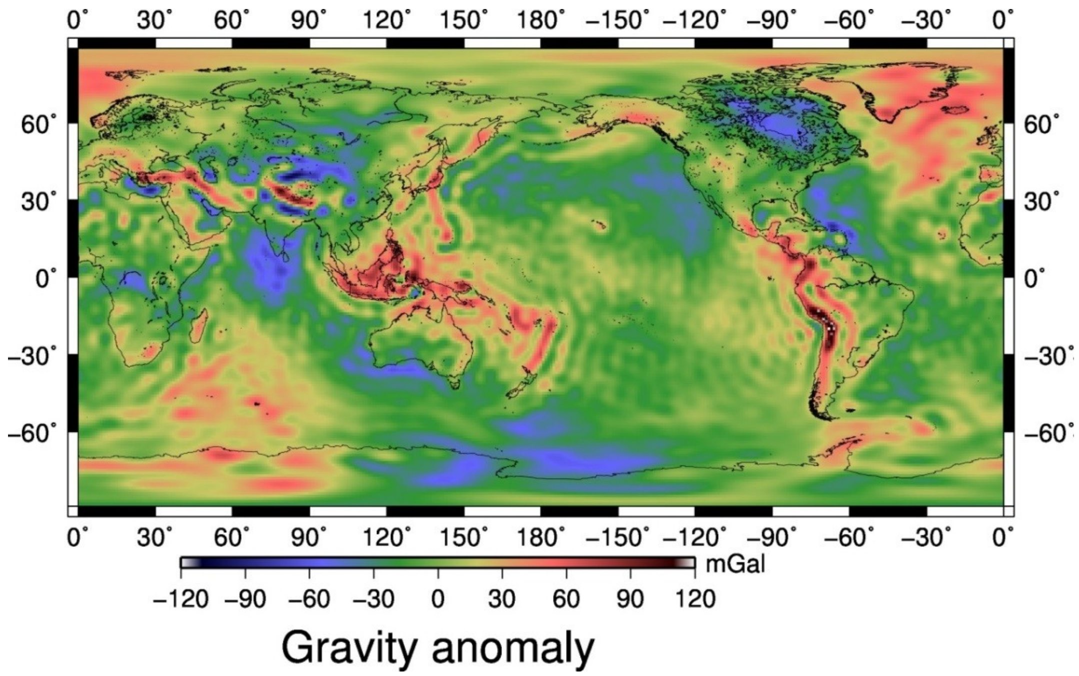

Figure 2.3 The map of the static gravity anomaly of the earth in November 2013 calculated from Level-2 GRACE data. I removed the C_{20} and C_{00} components.

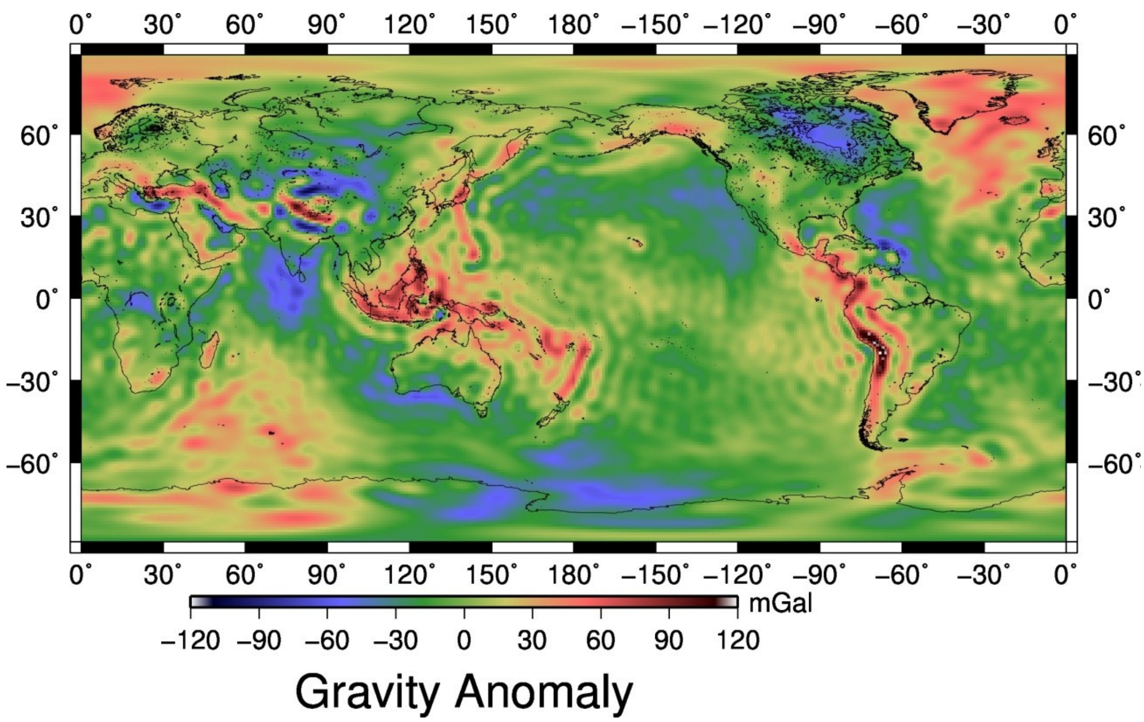

Figure 2.4 The map of the static gravity anomaly of the earth in October 2013 calculated from Level-2 GRACE data. I removed the C_{20} and C_{00} components. This looks almost identical to Figure 2.3.

Figures 2.3 and 2.4 show the gravity anomaly in November and October, respectively. They represent different time epochs, but they look alike because the temporal changes of the gravity fields are small. In order to study time-variable gravity, we have to use the unit of μGal. Figure 2.5 shows the difference of the gravity fields in November 2013 from October 2013.

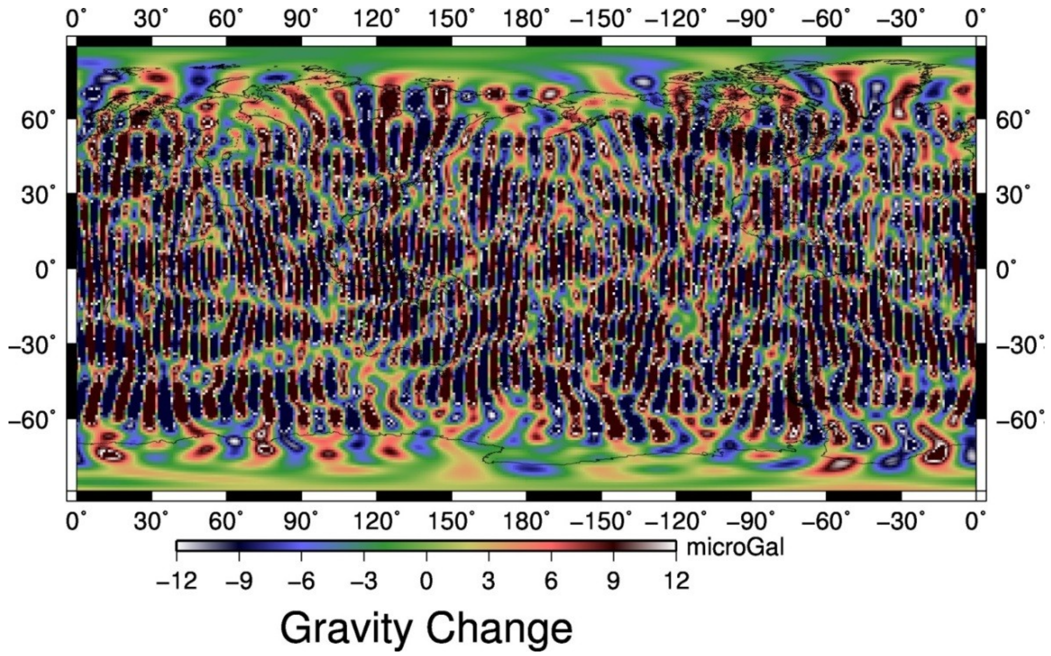

Figure 2.5 The gravity fields in November relative to those in October 2013.

Figure 2.5 shows the strong north-south stripes. These stripes appear because GRACE data are noisy in short-wavelength components; GRACE satellites orbit the earth in a polar circular orbit at the altitude of about 500 km, taking about 90 minutes per one cycle (they experience about 550 revolutions every month). This suggests that we have to take certain means to analyze (e.g. applying special filters) time variable gravity with the GRACE data.

One way to avoid these stripes is to use northward components rather than the downward component of the gravity field. The north components do not show the stripes because the GRACE satellites move in the north-south direction. We can calculate this by differentiating the gravity potential with respect to the latitude. Figure 2.6 shows the distribution of the northward component of the gravity changes between October and November, 2013.

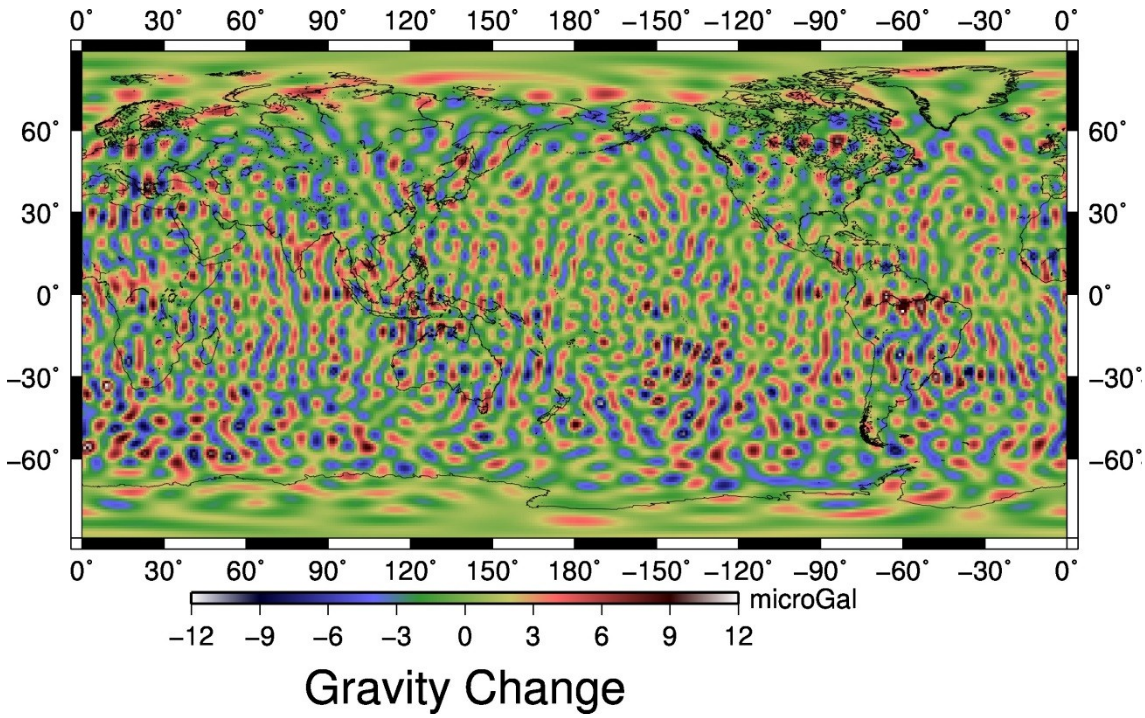

Figure 2.6 The northward component of the gravity changes from October to November in 2013. Strong north-south stripes in Figure 2.5 have disappeared.

The northward gravity changes observed with GRACE satellites are shown in Figure 2.6. They are largely free from strong stripes although short wavelength noises still remain. After all, we have to apply additional filters to GRACE data.

2.2 Spatial filters

2.2.1 De-striping filter

The filter to remove stripes is called de-striping filter proposed by *Swenson and Wahr* [2006]. They found that the stripes come from the highly systematic behavior of the Stokes' coefficients in the GRACE data. The Stokes' coefficients of C_{n16} are shown in Figure 2.7 as an example. There the red points (the evens of coefficients) are always bigger than blue points (odds) when *n* is larger than 30 and black line connecting them goes zigzag strongly. *Swenson and Wahr* [2006] considered that this is responsible for the stripes, and tried to suppress the stripes by getting rid of this systematic behavior. To do that, two polynomial functions were fitted with the least-squares method to each evens and odds of coefficients separately, and residuals between the values of original data and the fitted polynomial were taken as the new "de-striped" coefficients. Figure 2.8 shows the gravity change calculated with the de-striped coefficients. This de-striping filter is called as P5M10, which means that polynomials of degree 5 were fitted to the coefficients of degrees and orders 10 or more.

In this section, the gravity changes were calculated at first and then the de-striping filter was given because this order makes sense to understand the de-striping filter. Practically, the de-striping filter is applied to the data at first, and then the gravity changes are calculated to obtain the time series.

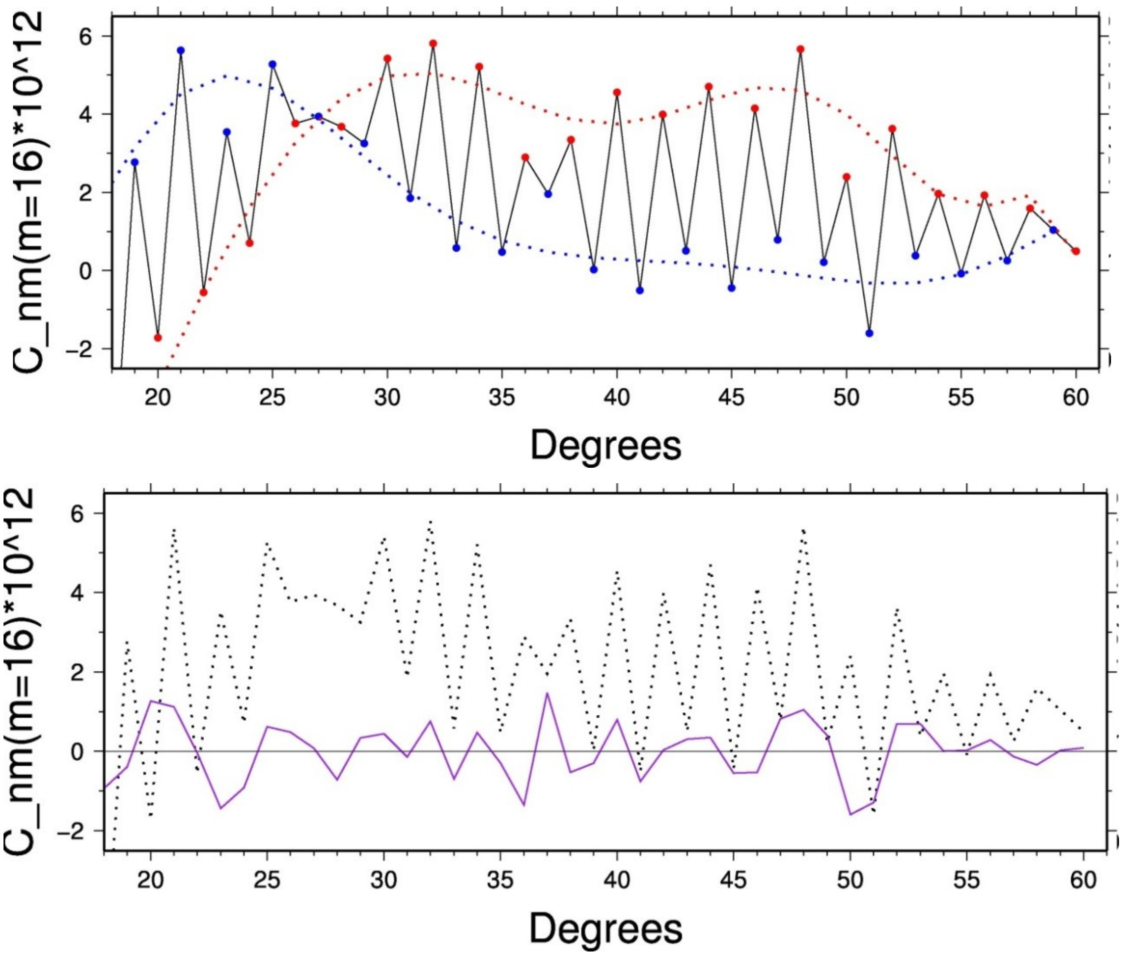

Figure 2.7 This figure gives conceptual explanation of the de-striping filter. (above) The solid black line indicate the Stokes' coefficients of order 16, i.e. ΔC_{n16} (C_{n16} in November 2013 – C_{n16} in October 2013) as a function of degree *n*. The red points denote the values of coefficients with even *n* and blue points denote those with odd *n*. The broken lines are the curves fitted to each color's data with polynomial degrees = 10. (below) The broken black line is the same line of the solid black line above. The purple line shows the difference between the black line and the fitted polynomial curves. The horizontal straight line means zero.

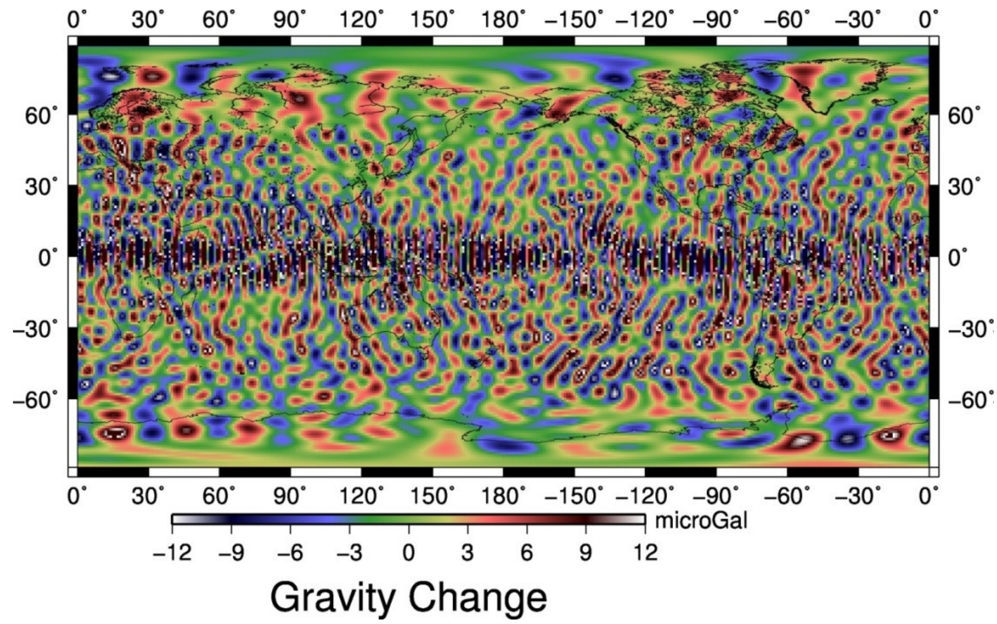

Figure 2.8 The gravity change in from October to November 2013 calculated with the "de-striped" coefficients.

Figure 2.8 shows that the de-striping filter effectively suppressed longitudinal stripes to a certain extent. However, it is not sufficient, and so the coefficients need to be further filtered as described in the next section (even the northward component data have to be filtered in the same way).

2.2.2 Fan filter

The best filter to make the spatial distribution of gravity change smooth is the two-dimensional Gaussian filter, called Fan filter [*Wahr et al.*, 1998; *Zhang et al.*, 2009]. The definition of this filter and how to apply it to the coefficients are shown with equations (2.2) ~ (2.6).

$$\Delta g(\theta, \varphi) = \frac{GM}{R^2} \sum_{m=2}^{nmax} (n-1) W_n \sum_{m=0}^{n} W_m (\Delta C_{nm} \cos m\varphi + \Delta S_{nm} \sin m\varphi) \overline{P_{nm}}(\sin\theta) \tag{2.2}$$

$$W_0 = 1 \tag{2.3}$$

$$W_1 = \frac{1+e^{-2b}}{1-e^{-2b}} - \frac{1}{b} \tag{2.4}$$

$$W_{n+2} = -\frac{2n+1}{b} W_{n+1} + W_n \tag{2.5}$$

$$b = \frac{\ln(2)}{(1-\cos\frac{r}{R})} \tag{2.6}$$

where W_n and W_m are the weighting function with Gaussian distribution at degree *n* and *m*, and *r* is the averaging radius. Weights with different *r* are shown in Figure 2.9.

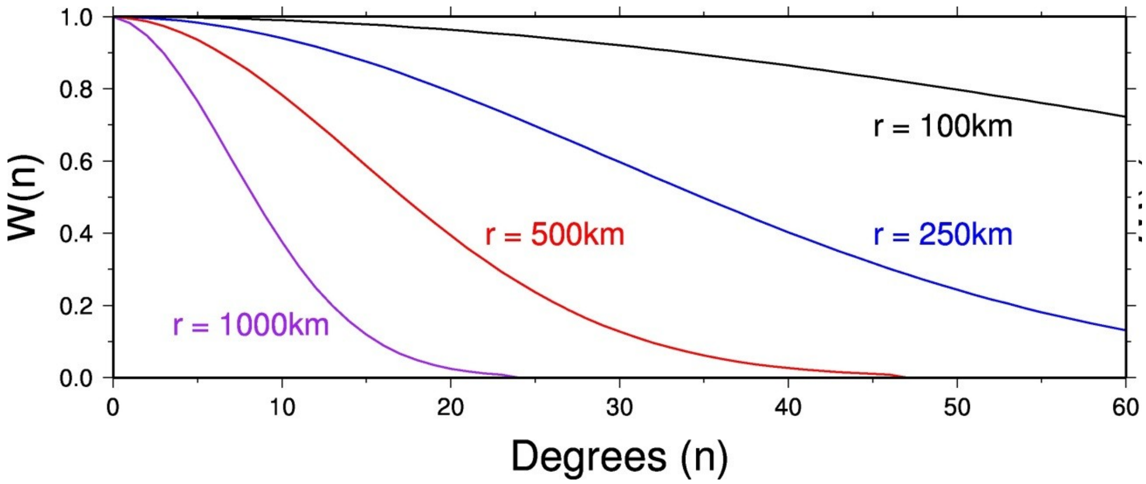

Figure 2.9 The values of *W*(*n*) as a function of degree *n* for the different values of *r*, i.e. 100 km, 250 km, 500 km, and 1000 km. For larger degrees, the weight becomes smaller.

Figure 2.9 shows that the fan filter gives smaller weights to coefficients of higher degree and order. That is why the shortwave noises are reduced by this filter. The gravity changes from October to November 2013 calculated with GRACE data after the de-striping filter and the fan filter are shown in Figure 2.10.

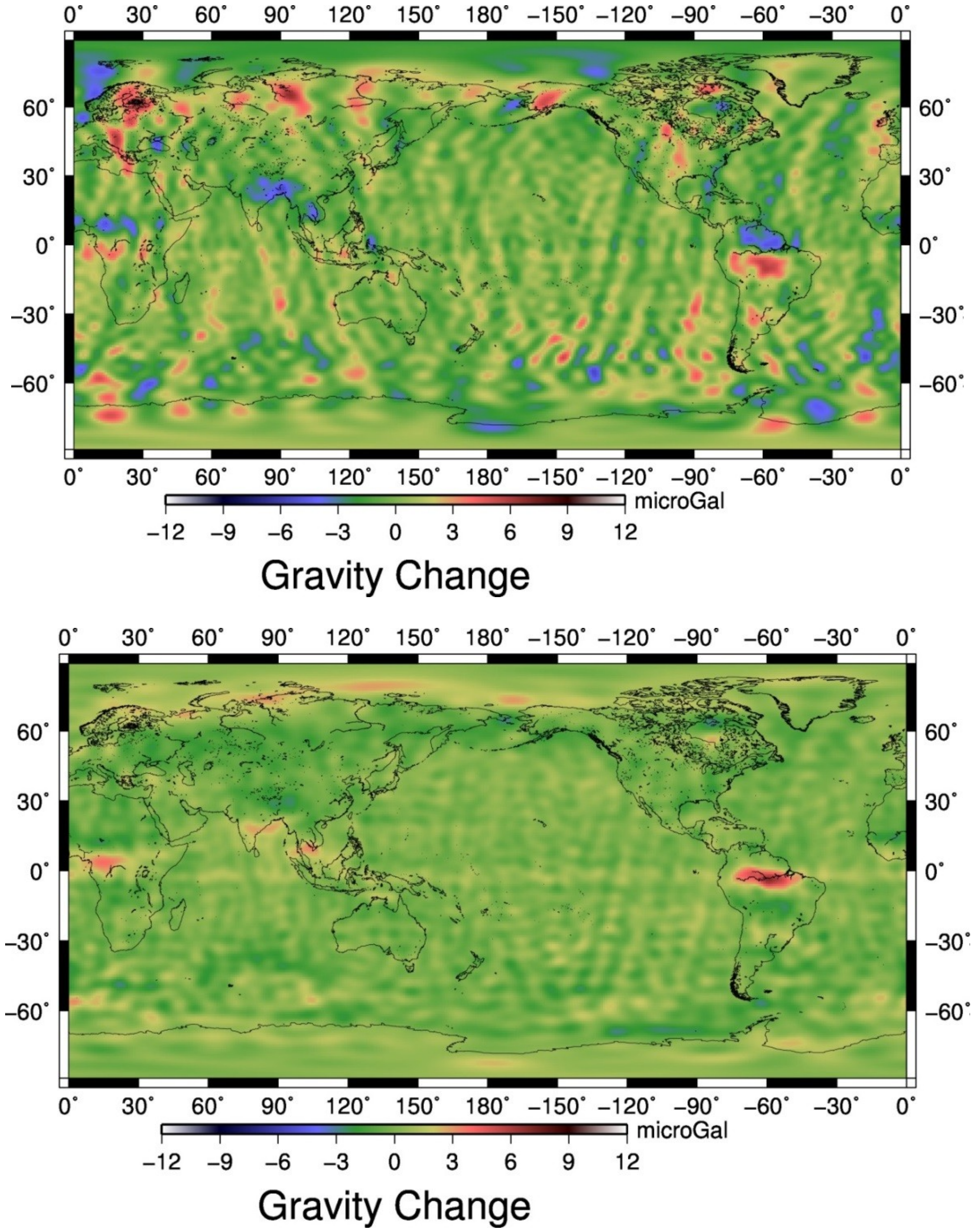

Figure 2.10 The gravity changes from October to November 2013. (above) The downward components of gravity change calculated from GRACE data with both de-striping (P3M15) and Fan filter (r = 250km). (below) The northward components of gravity change calculated from GRACE data with Fan filter (r = 250km).

2.3 GLDAS model

In this study, GLDAS Noah model [*Rodell et al.*, 2004] is used to remove the contribution of land hydrology to gravity. GLDAS model is made from the observed data of precipitation, temperature, and so on, and given as monthly values at 1×1 degree grid points, except for Antarctica and Greenland. The data give the amount of water (kg/m^2) there, so it has to be changed into spherical harmonic coefficients and into those of gravity by formulations given in *Wahr et al.* [1998]. They are filtered in the same way to de-stripe and reduce short-wavelength noises as for the GRACE data. Before converting to spherical harmonic coefficients, grid values in Greenland/Antarctica were set to zero.

2.4 Time series analysis

The function (2.7) is fitted to the GRACE data with the least-squares method to estimate the postseismic gravity changes and the function (2.8) is used to get the time series of gravity deviations by eliminating components not related to earthquakes.

$$G = a + bt + c\,sin(\omega t + \theta_1) + d\,sin(2\omega t + \theta_2) + H(t)\left\{\Delta g + \sum_i e_i \times f_i(\Delta t)\right\} \tag{2.7}$$

$$\hat{G} = G - \{\, bt + c\sin(\omega t + \theta_1) + d\sin(2\omega t + \theta_2)\,\} \tag{2.8}$$

There $f_i\,(\Delta t)$ are certain functions to be fitted to the time-decaying components after the earthquakes and the others in (2.7) are the same as (1.1). $\hat{G}$ is the gravity changes obtained by removing the secular and seasonal components. We will discuss what kind of $f_i(\Delta t)$ best models the postseismic gravity changes in the chapter of results and discussion.

2.5 Model calculation

The software package by *Sun et al.* [2009] is used to calculate coseismic gravity changes together with fault parameters shown in *Banerjee et al.*, [2005] for the 2004 Sumatra-Andaman earthquake, *Heki and Matsuo* [2010] for the 2010 Chile (Maule) earthquake, and *Matsuo and Heki* [2011] for the 2011 Tohoku-oki earthquake.

The contribution of sea water to gravity also has to be added because *Sun et al.* [2009] gives the amount of gravity changes on “dry” earth, which has no water on it. The earthquakes give the surface of the earth deformation and it makes the sea water move, so the observed gravity changes have contributions of both dry earth and sea water. The correction is simply achieved by assuming the gravity field made by thin sea water layer as deep as the vertical crustal movements.

3 Results and discussion

3.1 Re-analysis of postseismic gravity changes of the 2004 Sumatra-Andaman earthquake.

I re-analyzed the postseismic gravity changes of the 2004 Sumatra-Andaman earthquake with newer data (Release 05) than those used in *Ogawa and Heki* [2007] (Release 02) with the equation (1.1), and found that the gravity had decreased for a few months after the earthquake and increased slowly after that. This behavior cannot be modeled with the equation (1.1) because the component there for postseismic gravity changes is expressed only with one exponential function, which is used for long-term increasing (the red curve in Figure 3.1). Therefore, we gave one more exponential function term to the equation (equation (3.1)), so that both the short- and long-term postseismic gravity changes are expressed with the model (the blue curve in Figure 3.1). This finding encouraged us to examine gravity changes of other large earthquakes. It is also important to compare two-dimensional distribution of postseismic gravity changes of these two components. Hence, we analyzed the gravity change time series of not only the 2004 Sumatra-Andaman earthquake, but also the 2010 Chile (Maule) earthquake and the 2011 Tohoku-oki earthquake.

$$G = a + bt + c\sin(\omega t + \theta_1) + d\sin(2\omega t + \theta_2)$$

$$+H(t)\left\{\Delta g + e_1\left(1 - \exp\left(\frac{\Delta t}{\tau_1}\right)\right) + e_2\left(1 - \exp\left(\frac{\Delta t}{\tau_2}\right)\right)\right\} \qquad (3.1)$$

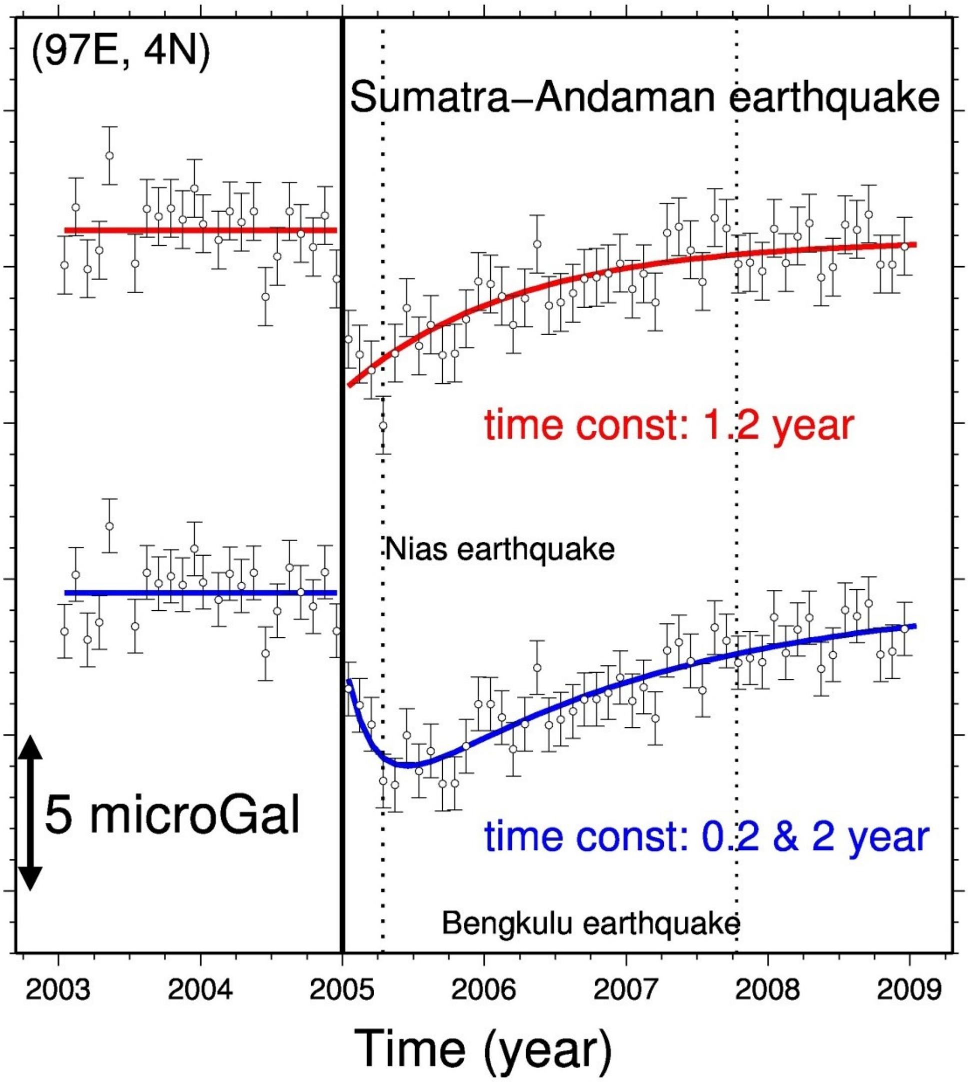

Figure 3.1 Time series of gravity changes before and after the 2004 Sumatra-Andaman earthquake at a point (4N, 97E), shown in Figure 3.2, fitted with two different models. The white circles are the time series after removing seasonal and secular gravity changes and the steps at the 2005 Nias earthquake and 2007 Bengkulu earthquake. The vertical lines indicate the occurrences of three earthquakes. The red and blue curves are fitted with the postseismic gravity change modeled with only one component (τ=1.2 year) and with two components (τ_1=0.2 year and τ_2=2 year), respectively. The gravity decrease immediately after the earthquake is well modeled only with the blue curve.

3.2 Co- and postseismic gravity changes of three Mw9-class earthquakes

3.2.1 Vertical gravity changes (Observed and calculated)

3.2.1.1 Coseismic gravity changes

In Figure 3.2 we compare the geographic distributions of coseismic, and short- and long-term postseismic gravity changes of the three megathrust events. The signal-to-noise ratio is not good especially for the Maule earthquake due to the relatively small magnitude and large land hydrological signals. In fact, this area is known to have experienced a drought in 2010. The removal of hydrological signals by GLDAS did not work well enough in this region (Figure 3.3) due possibly to insufficient meteorological observation data to be put into the GLDAS models. Nevertheless, fairly systematic gravity signals are seen near the epicenter.

Figure 3.2 (a-1, b-1, and c-1) shows that the coseismic signatures of the three cases are dominated by gravity decreases on the back arc side of the fault with smaller increases on the fore arc side. The latter are often attenuated by the existence of seawater [*Heki and Matsuo*, 2010]. Such coseismic changes are well understood with the theory discussed in Section 1.3. The coseismic signature, after spatial filtering, appears as the gravity decrease on the back arc side of the arc [*Han et al.*, 2006].

The observed and calculated coseismic gravity changes are compared in Figures 3.5-3.7. In the model calculation, I used the software package by *Sun et al.* [2009] and fault parameters from other references, as described in Section 2.5. Each case shows certain difference between the observation and the calculation, but the two patterns are more or less consistent suggesting that the theoretical model is realistic enough.

3.2.1.2 Postseismic gravity changes

The middle column of Figure 3.2 suggests that the short-term postseismic gravity changes also show negative polarities, although their centers seem to shift a little from back-arc regions toward trenches. On the other hand, the long-term postseismic gravity changes (the right column of Figure 3.2) have positive polarities and occur directly above the ruptured fault. These features are common in the three earthquakes.

The elastic response to the afterslip should occur as the continuation of the coseismic gravity changes. The distribution of the postseismic gravity changes by the afterslip of the 2011 Tohoku-oki earthquake is shown in Figure 3.8, which was calculated with the software of *Sun et al.* [2009] from the afterslip distribution shown in Figure 3.9 inferred from GPS data. They are both dominated by negative changes. However, the trenchward shift of the center is seen, and this cannot be explained simply by the down-dip migration of the slip [*Ozawa et al.*, 2012]. In addition to that, the time constant of the short-term postseismic gravity change of the 2011 Tohoku-oki earthquake (0.1 year) is different from the afterslip (0.4 year in *Ozawa et al.* [2012], although the mathematical model to express the postseismic change is different from ours).

The long-term postseismic gravity changes may reflect multiple processes possibly except for afterslip. So far, several mechanisms have been proposed for the postseismic gravity changes, e.g. viscous relaxation of rocks in the upper mantle [*Han and Simons*, 2008; *Panet et al.*, 2007; *Tanaka et al.*, 2006; *Tanaka et al.*, 2007], diffusion of supercritical water around the down-dip end of the ruptured fault [*Ogawa and Heki*, 2007].

The viscoelastic mantle relaxation can play a major role in the long-term postseismic gravity changes. Figure 3.10 shows the postseismic gravity changes for two years from observation and from calculation on viscoelastic postseismic deformation with the method of *Tanaka et al.* [2006; 2007]. This figure suggests that the mantle relaxation has the strong possibility to explain postseismic gravity changes.

However, this does not necessarily rule out other possibilities, and also has a problem that the viscoelastic relaxation normally takes a longer time (10 years or more) because of the high viscosity of rocks in the upper mantle. The average viscosity in the upper mantle at ~100 km depth is more than 10^{20} (Pa s) [*Fei et al.*, 2013] while the calculation results in Figure 3.10 assumes the viscosity of 3×10^{18} (Pa s). I had to assume such a small viscosity to explain the long-term postseismic gravity changes with the viscoelastic mantle relaxation. Even if the mantle under the faults of 2004 Sumatra-Andaman earthquakes are much softer than the average, the long-term postseismic gravity changes of the 2010 Chile (Maule) earthquake and the 2011 Tohoku-oki earthquake take only a few months for the gravity to start increasing. It is not realistic that all of the viscosities of the rocks under the faults of the three megathrust earthquakes are much lower than average. Viscoelastic mantle relaxation has strong possibility that it plays an important role of long-term postseismic gravity changes but it cannot explain them completely.

The diffusion of supercritical water around the down-dip end of the ruptured fault can explain the postseismic gravity increase in the relatively short timescale to some extent, but there have been no decisive evidence to prove or disprove it. And there is another problem: the diffusion of supercritical water does not explain the distribution of the changes, i.e. they occur directly above the rupture area.

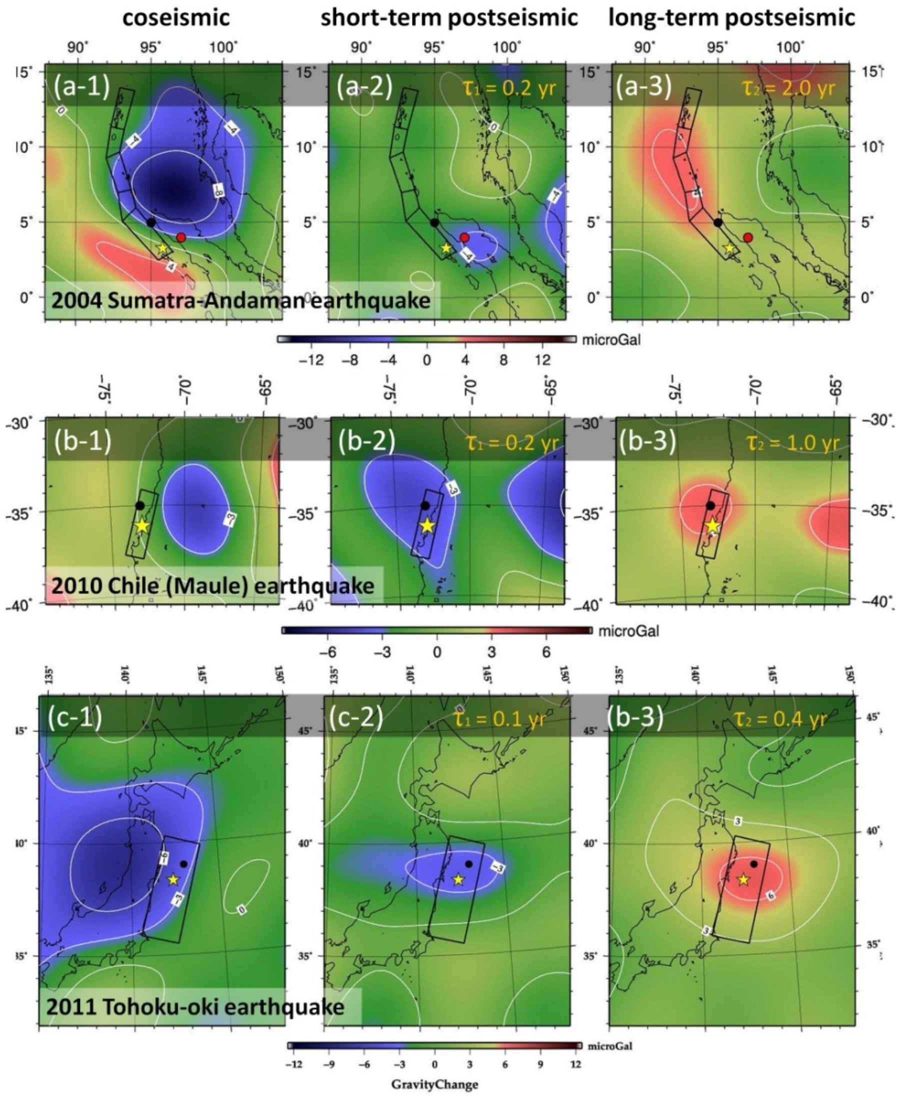

Figure 3.2 Coseismic (left), and short-term (middle) and long-term (right) postseismic gravity changes of the three M9 class earthquakes, i.e. the 2004 Sumatra-Andaman (a), the 2010 Maule (b), and the 2011 Tohoku-Oki (c) earthquakes. The postseismic gravity changes are expressed with 2 year (the 2004 Sumatra-Andaman) and 1 year (the other two earthquakes) cumulative changes. Time constants are shown on the figure. The yellow stars and black squares show the epicenters and the approximate shapes of the faults that slipped in the earthquakes. The red circles in (a) and the black circles in in (a), (b), and (c) show the points whose gravity time series are shown in Figure 3.1 (red circles) and in Figure 3.4 (black circles). The contour intervals in (a), (b), and (c) are 4 μGal, 3 μGal, and 3 μGal, respectively. The gravity show coseismic decreases, then keep decreasing for a few months (short-term postseismic). It then increases slowly (long-term postseismic) with slightly different spatial distribution from the other two components.

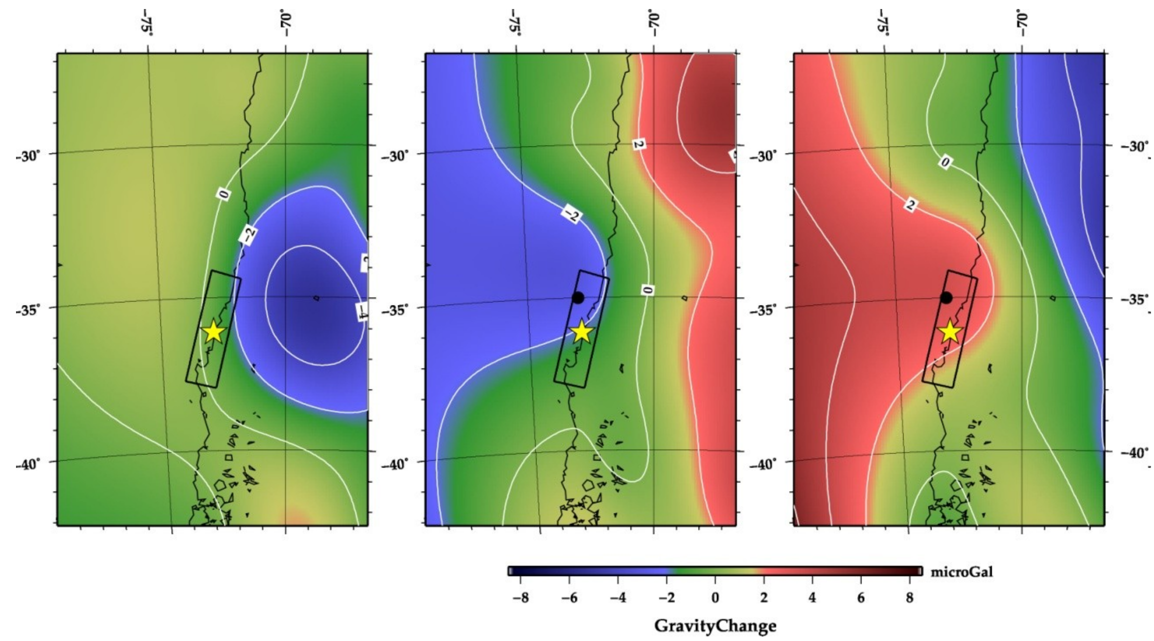

Figure 3.3 Co- (left) and postseismic (middle and right) gravity changes calculated with GRACE data and GLDAS model. There is no improvement in the postseismic gravity changes by considering land hydrological contribution with the GLDAS model (middle and right).

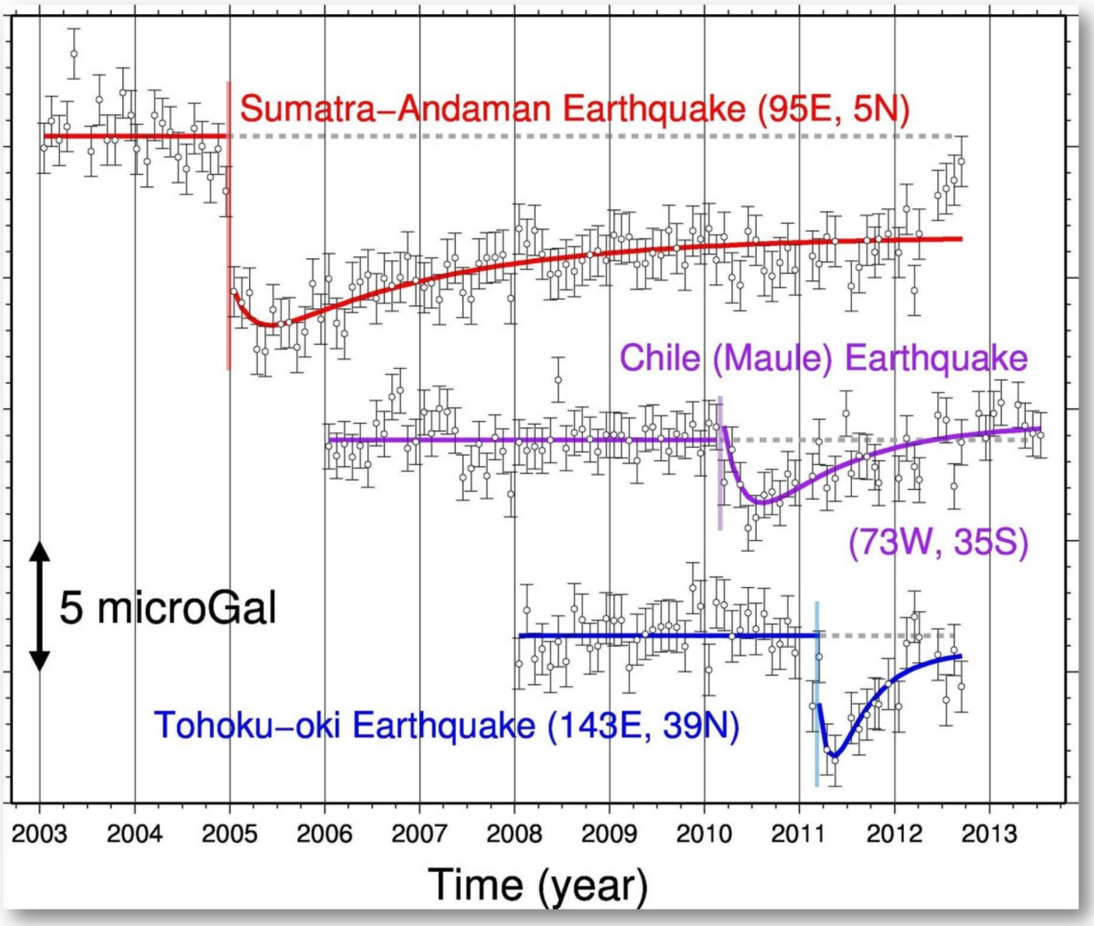

Figure 3.4 Time series of gravity changes before and after the three megathrust earthquakes at the black circles shown in Figure 3.2. The white circles are the data whose seasonal and secular changes were removed. The vertical translucent lines denote the earthquake occurrence times. All the three earthquakes suggest the existence of two postseismic components in gravity changes with opposite polarities and distinct time constants.

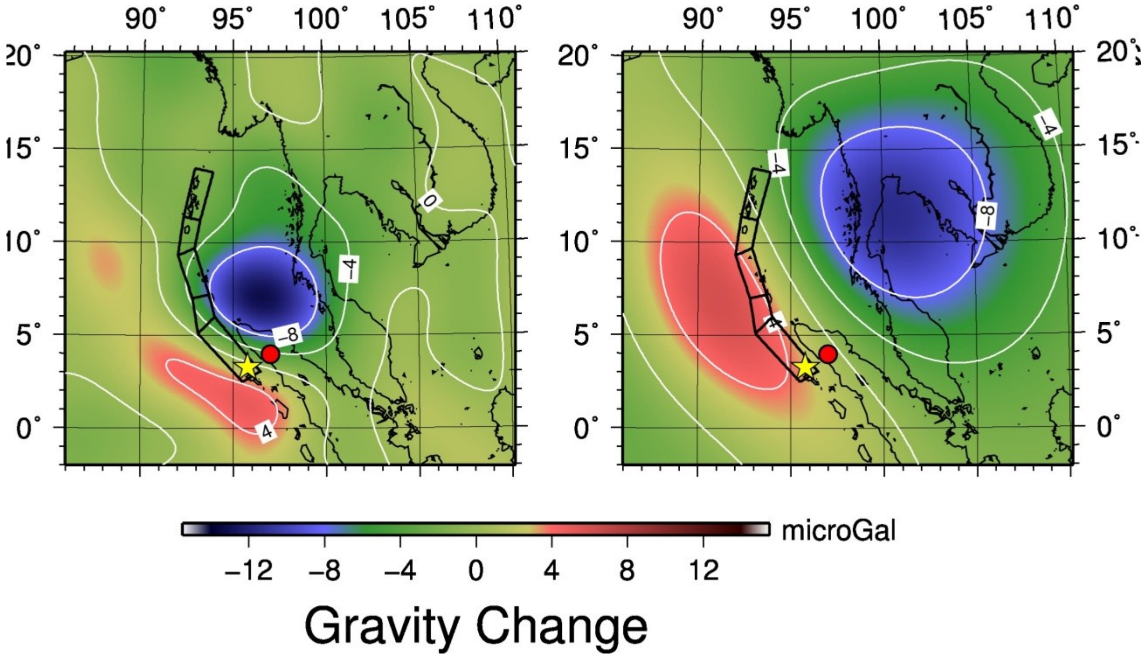

Figure 3.5 The distribution of observed coseismic gravity changes of 2004 Sumatra-Andaman earthquake (left) and those calculated with the software of *Sun et al.* [2009] and the fault model of *Banerjee et al.* [2005] (right) as described in Section 2.5. The amounts of gravity changes are nearly consistent but the spatial pattern is significantly different. This may suggest the fault model is not so good to explain the coseismic gravity change.

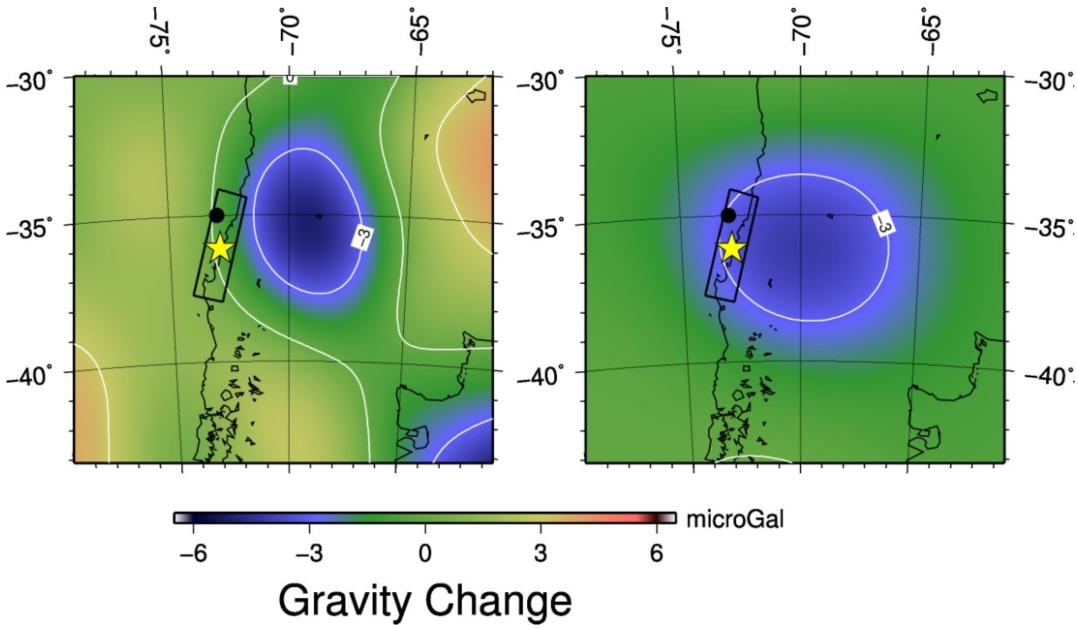

Figure 3.6 The distribution of the observed coseismic gravity changes (left) of the 2010 Maule earthquake and those calculated with the software of *Sun et al.* [2009] and the same fault model as used in *Heki and Matsuo* [2010] (right). The two patterns are similar to each other. The black squares, yellow stars, and black points are the same as in Figure 3.2.

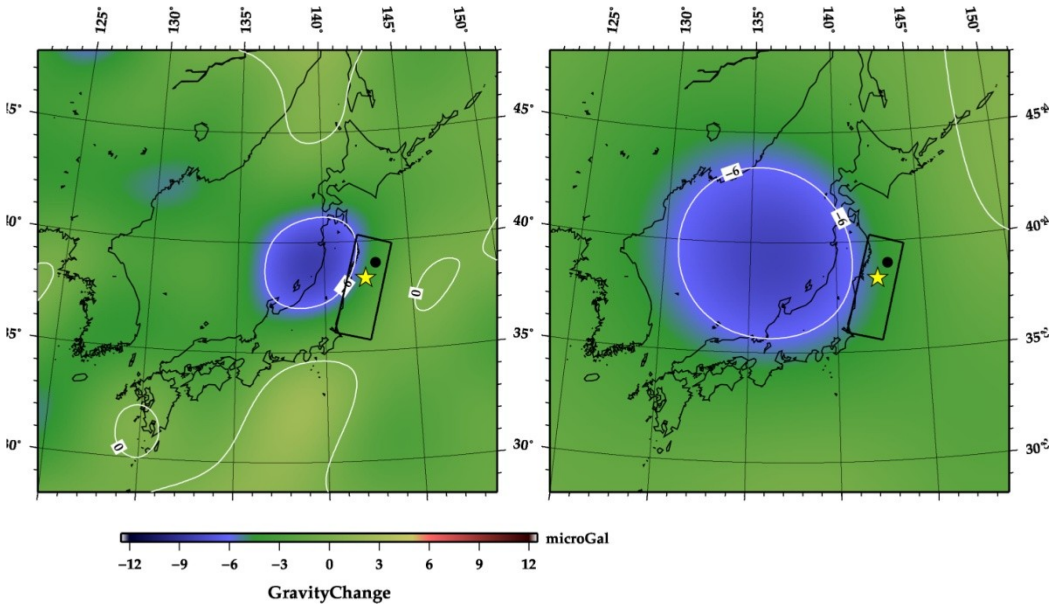

Figure 3.7 The distribution of observed coseismic gravity changes (left) of the 2011 Tohoku-oki earthquake and those calculated with the software of *Sun et al*. [2009] and the same fault model as in *Matsuo and Heki* [2011] (right). The two figures are similar to each other to a certain extent. The black squares, yellow stars, and black points are the same as in Figure 3.2.

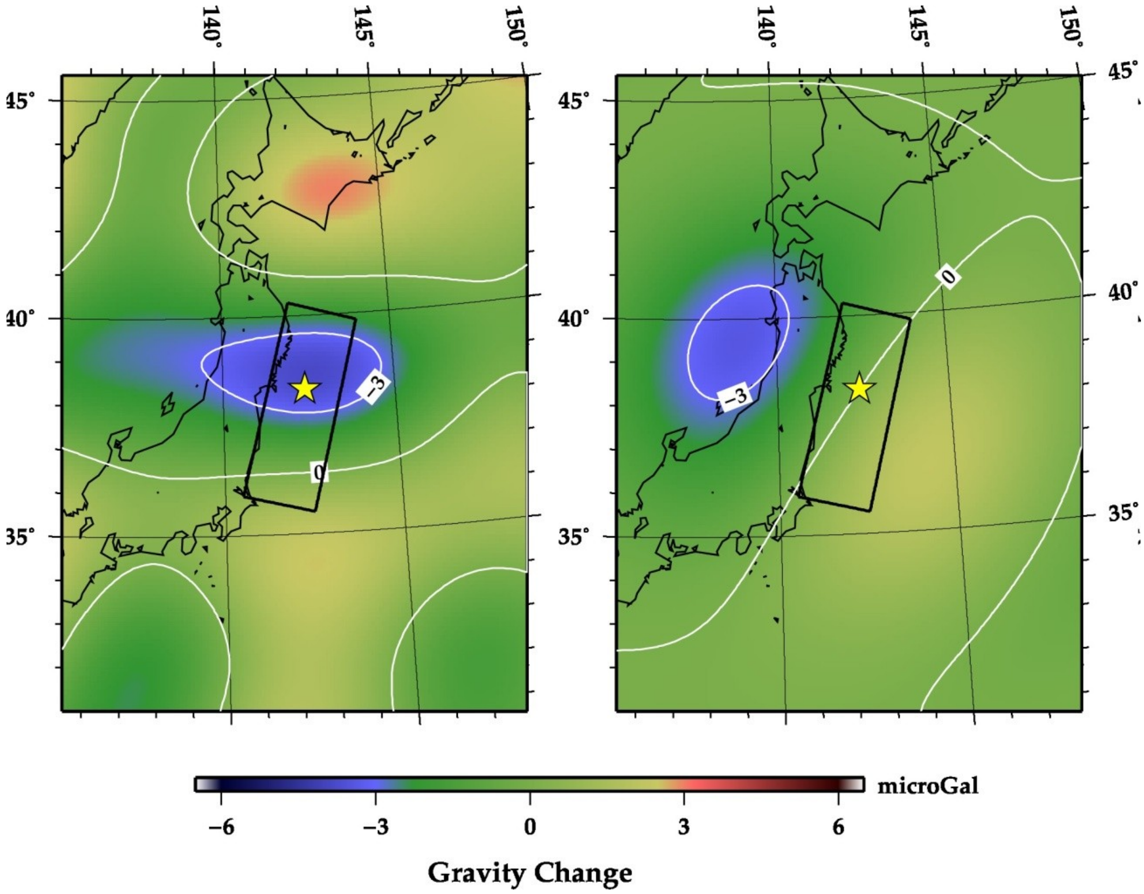

Figure 3.8 (left) The same figure as Figure 3.2c-2 (right). The gravity changes of the afterslip calculated with the slip distribution inferred from GPS data shown in Figure 3.9 [*Koji Matsuo*, personal communication]. The amplitudes of gravity changes are consistent but there are significant differences in their spatial patterns.

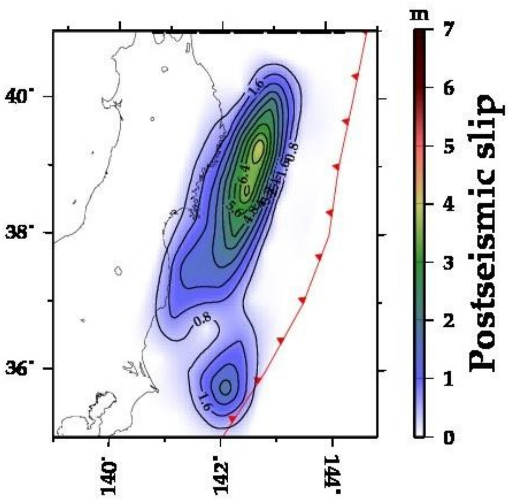

Figure 3.9 The slip distribution of the afterslip of 2011 Tohoku-oki earthquake inferred from GPS data [*Koji Matsuo*, personal communication].

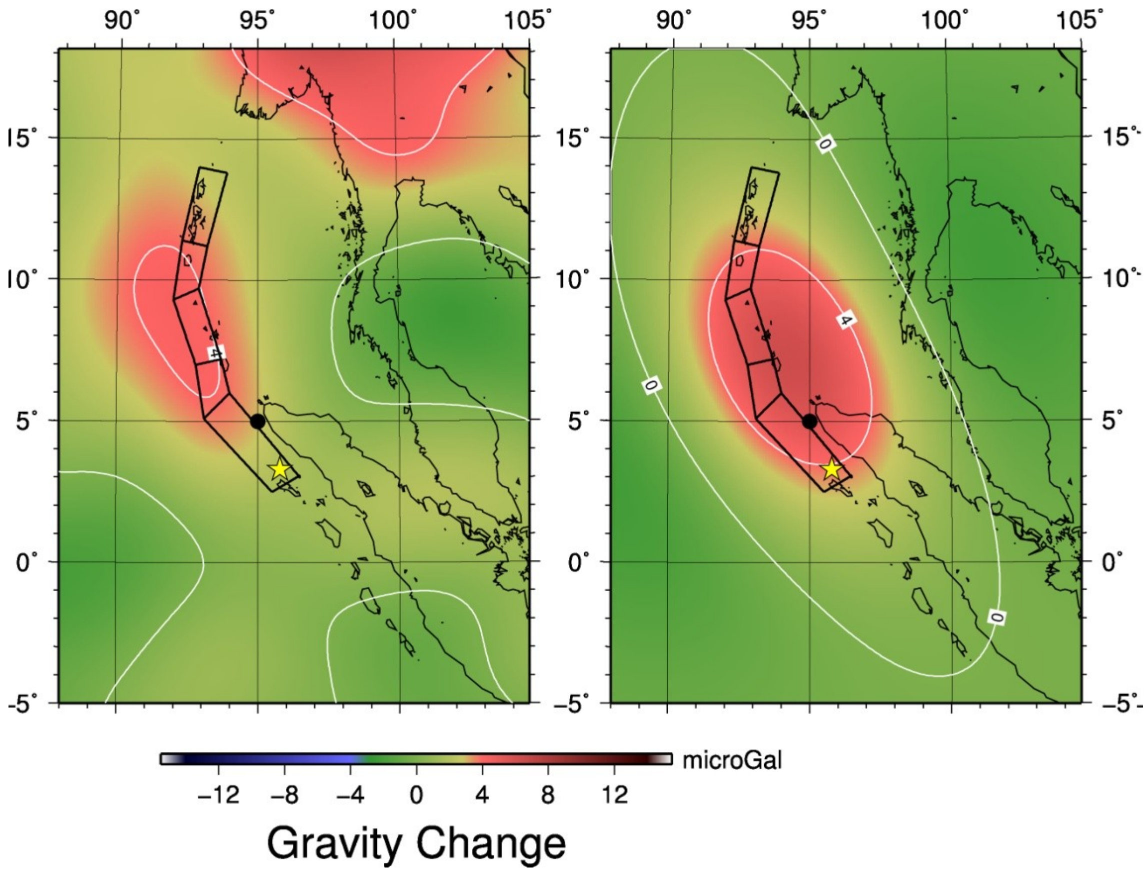

Figure 3.10 (left) The same figure as Figure 3.2a-3. (right) The gravity changes of the viscoelastic mantle relaxation calculated with the viscosity of 3×10^{18} (Pa s) by *Yoshiyuki Tanaka* [personal communication], based on the algorithm of *Tanaka et al*. [2006; 2007]. Both of the amounts and spatial patterns of gravity changes are similar to each other.

Next I perform the F-test to see if the two postseismic gravity change components are statistically significant. The F-test is a statistical test to infer the possibility that the scatters of two groups are the same. If this possibility is low enough, we can tell that the scatters of the two groups are different (i.e. one is significantly smaller than the other) with a certain confidence. In the next paragraph, I will briefly explain its procedure using equations (3.2) ~ (3.5).

At first, the short-term postseismic gravity changes are presumed to be noises. Then each data becomes independent because they are just noises, so F-test can be done. If F-test showed that the possibility of the coincidence is high, the hypothesis cannot be ruled out (i.e. the short-term changes would be only noises). If the possibility is low, the hypothesis is turned down (i.e. the short-term gravity changes would be real signals).

I compared the variances between the two cases, i.e. (1) one exponential function, and (2) two exponential functions with different time constants, at the black points in Figure 3.2 to do F-test.

$$\sigma^2 = \frac{\sum(x-\bar{x})^2}{n-1} \tag{3.2}$$

$$F = \frac{variance\ 1}{variance\ 2} = \frac{\sigma_1^2}{\sigma_2^2} \tag{3.3}$$

$$f(F,\emptyset_1,\emptyset_2) = \left(\frac{\emptyset_1}{\emptyset_2}\right)^{\frac{\emptyset_1}{2}} \frac{\Gamma(\frac{\emptyset_1+\emptyset_2}{2})}{\Gamma\left(\frac{\emptyset_1}{2}\right)\Gamma\left(\frac{\emptyset_2}{2}\right)} \frac{F^{\frac{\emptyset_1-2}{2}}}{\left(1+\frac{\emptyset_1}{\emptyset_2}F\right)^{\frac{\emptyset_1+\emptyset_2}{2}}} \tag{3.4}$$

$$\Gamma(z) = \int_0^\infty t^{z-1}e^{-t}dt, \tag{3.5}$$

where σ^2 is the variance (σ is the standard deviation), x_i are the values of data, $\bar{x}$ is the mean of x_i, n is the number of data x_i. $\emptyset$ is the degree-of-freedom of the data (= n – 1), and Γ is the gamma-function. The value f gives the possibility that the difference of variances of two groups is insignificant. In this study, the data x_i are observed gravity values and $\bar{x}$ corresponds to the fitted function (either one or two exponential functions).

The time constant for the case of single exponential function is determined so that the variance of the whole data set becomes minimal. However, the two time constants for the function with double exponential functions cannot be determined in this way because the inferred short- and long-term postseismic gravity changes become too much to be realistic (they become larger than coseismic gravity changes) with unrealistic spatial distributions (Figure 3.11). Though the mechanisms of postseismic gravity changes are not clear, this is obviously unreasonable. The time constants in the case of two exponential functions are determined subjectively so that the model fits the data well near the epicenters.

I tried three cases in which the data lengths were taken as twelve, eighteen, or twenty months after the earthquake. In all of these cases, unfortunately, the result of the F-test did not show that the variances in the two-exponential-function model are significantly smaller than the one-exponential-function model. This suggests that both of the models can approximate the long-term time series equally well from statistical point of view. Obviously, we need evidence other than F-test to claim the existence of the two component.

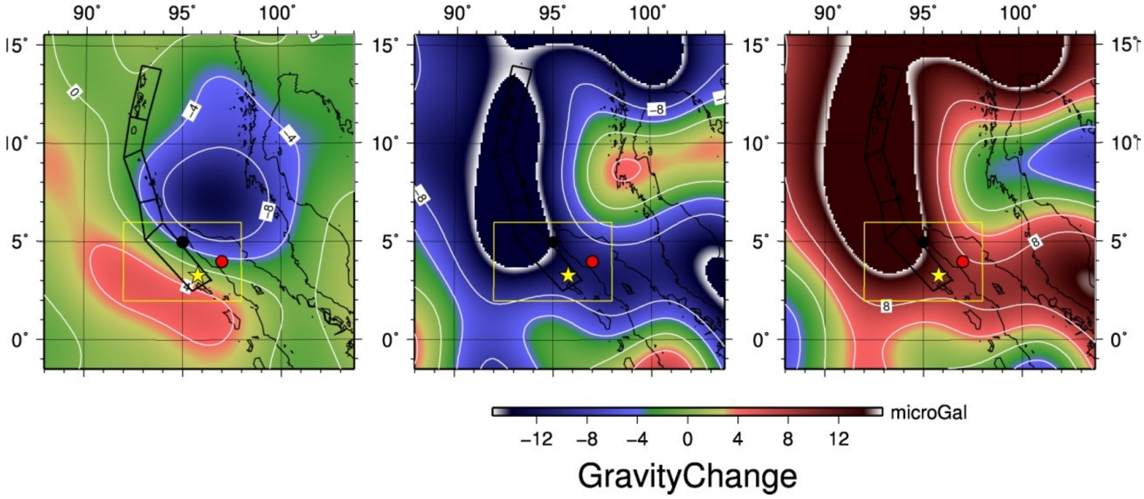

Figure 3.11 The gravity changes calculated with the time constants of 0.3 year and 0.4 year, which minimizes the variance within the yellow square after the earthquake. The area and the term are decided because short-term postseismic gravity changes are seen well there. The other marks are the same as Figure 3.2. Clearly, there are strong negative correlations between the short- and long-term postseismic gravity changes (which are much larger than coseismic gravity changes). When the yellow square is sifted, these distributions also change. These results are quite unrealistic, and the simple method to minimize the variance (or RMS) cannot be used to get two time constants.

3.2.2 Northward gravity changes (Observed)

The northward co- and postseismic gravity changes are also calculated from the GRACE data with the Fan filter (r = 250km) but <u>without</u> de-striping filter. They are shown in Figures 3.13-3.20. Coseismic gravity changes have northward components. However, the northward component is not so strong in the postseismic gravity changes (Figure 3.12). I also found that there are no significant differences between the variances of the fits with single-component and with two-components (long- and short-term components) (Figure 3.13). After all, monitoring of the north gravity component has a certain “stripe-free” benefit, but it may not provide additional information on the two components in the postseismic gravity changes.

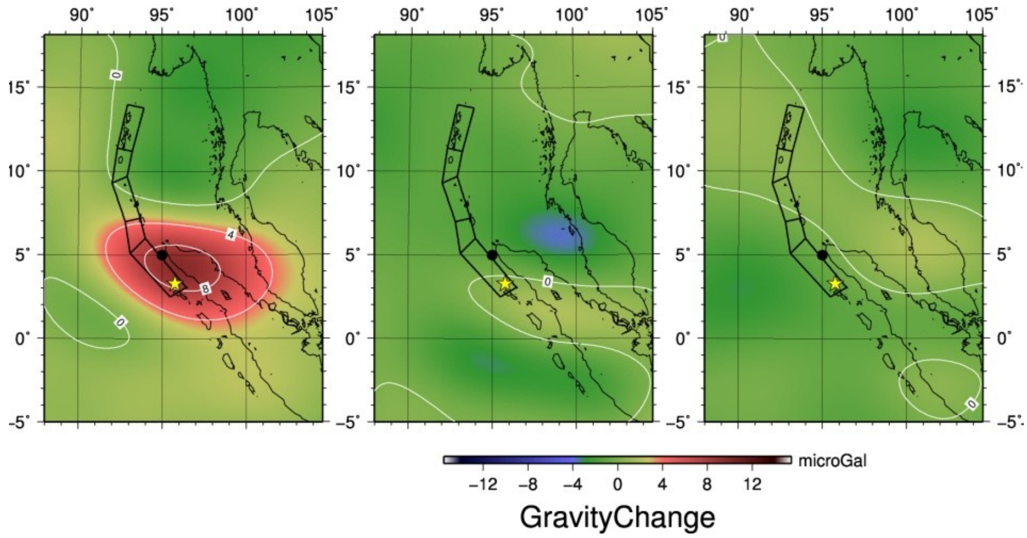

Figure 3.12 The co- (left) and short-term (middle) and long-term (right) postseismic changes in the northward gravity component associated with the 2004 Sumatra-Andaman earthquake. The all symbols are the same as Figure 3.2. The coseismic gravity change is fairly large but postseismic gravity changes are not so clear as in the vertical gravity component.

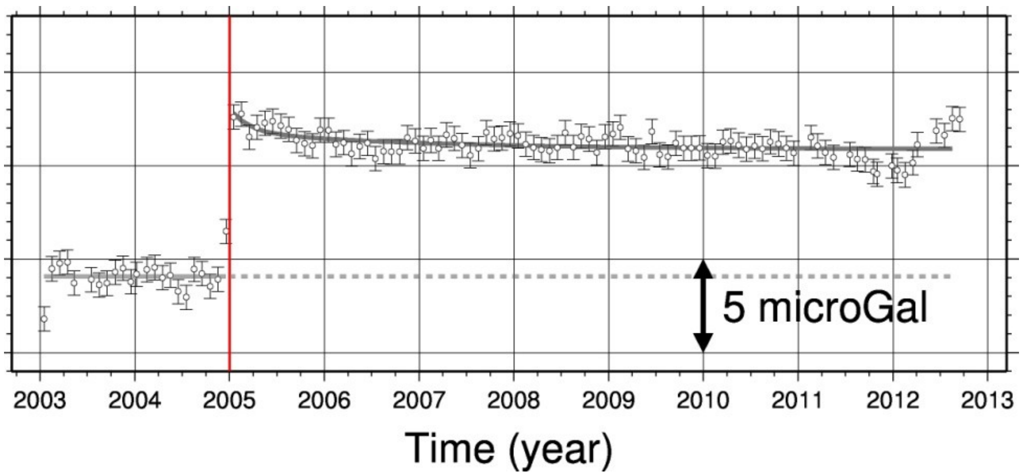

Figure 3.13 The time series of northward gravity changes of the 2004 Sumatra-Andaman earthquake at the point shown with a black circle in Figure 3.12 (95E, 5N). The gravity decreased a little after the earthquake, but the longer-term component is not clear in this time series.

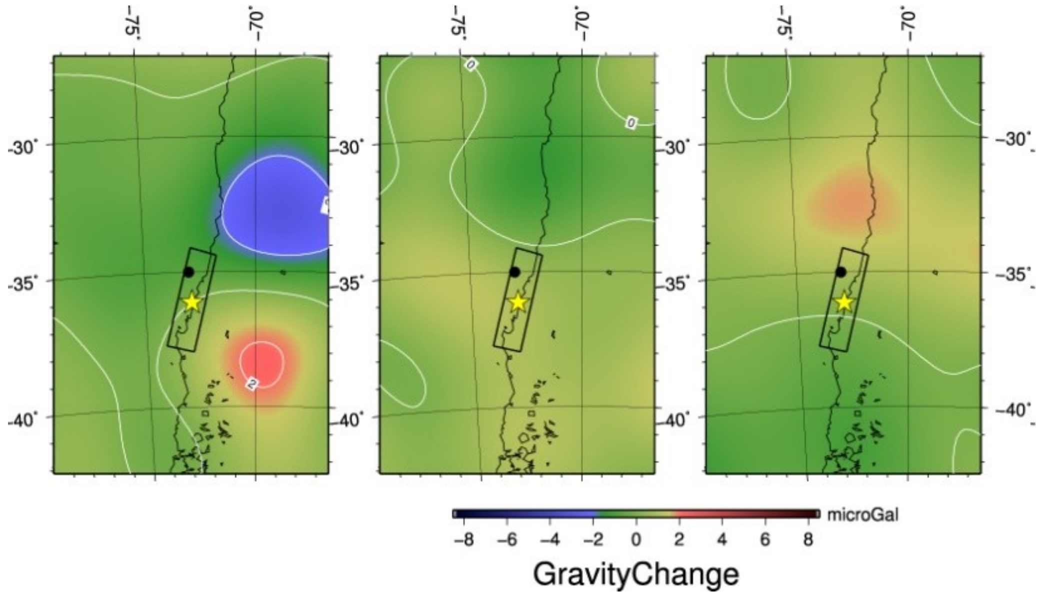

Figure 3.14 The co- (left) and short- (middle) and long-term (right) postseismic northward gravity changes of the 2010 Chile (Maule) earthquake. The all symbols are the same as Figure 3.2. Although the coseismic gravity changes are clear, postseismic gravity changes are not obvious.

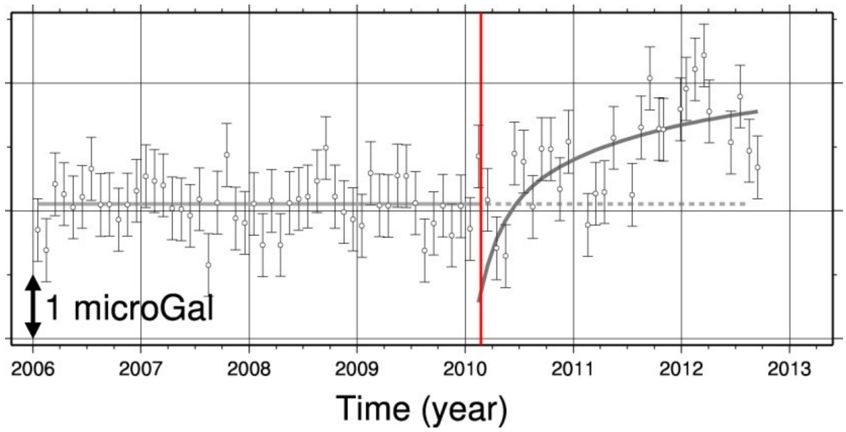

Figure 3.15 The time series of the northward gravity changes before and after the 2010 Chile (Maule) earthquake at the point shown with a black circle in Figure 3.14 (75W, 35S). Postseismic gravity change is seen well but this is not seen in Figure 3.14 because the postseismic gravity changes are modeled with only single exponential component.

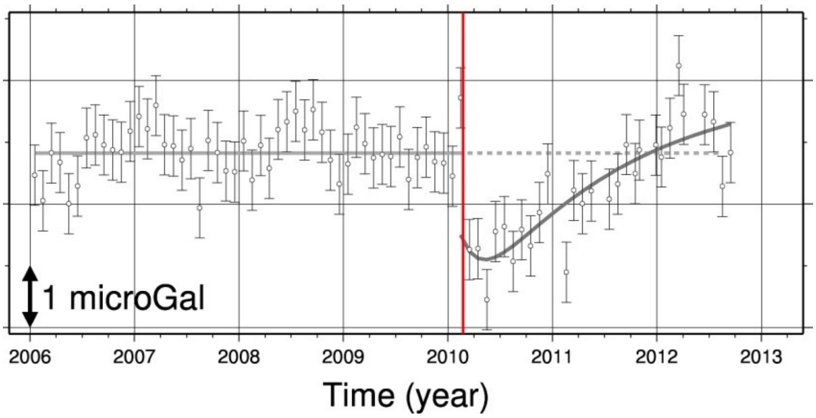

Figure 3.16 The time series of northward gravity changes before and after the 2010 Chile (Maule) earthquake at (72W, 33S), the center the region showing postseismic increase (bright red part) in Figure 3.14 (right). The short-term decreased over the first few months after the earthquake and long-term increase are seen, but they are not so clear as in the vertical component.

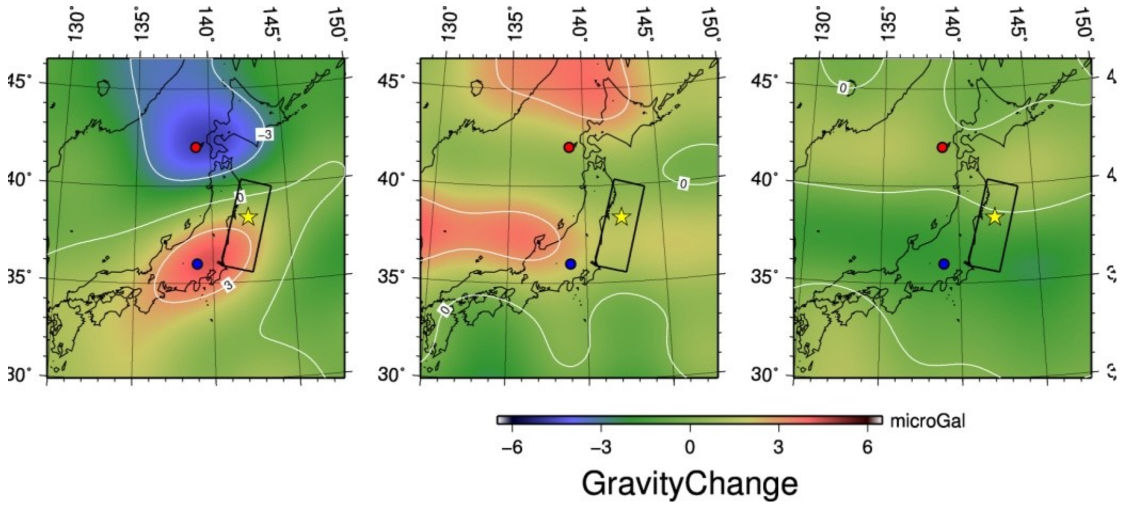

Figure 3.17 The co- (left) and short- (middle) and long-term (right) postseismic northward gravity changes of the 2011 Tohoku-oki earthquake. The all symbols are the same as Figure 3.2. Although the coseismic gravity changes are clear, postseismic gravity changes are not so clear as in the vertical component.

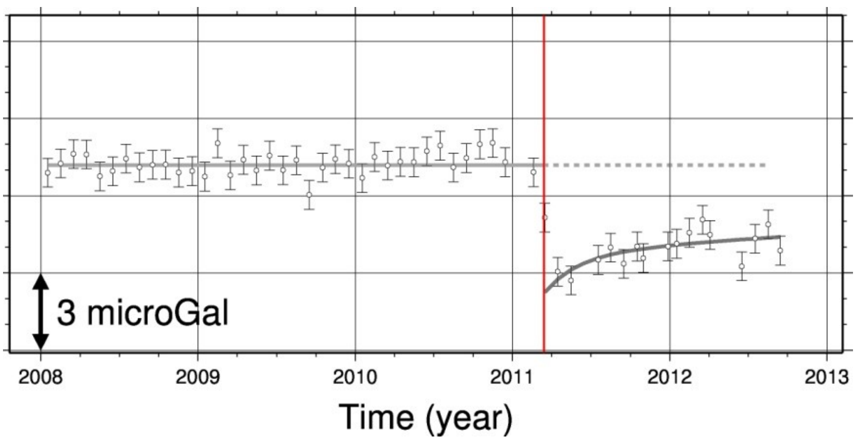

Figure 3.18 The time series of northward gravity changes before and after the 2011 Tohoku-oki earthquake at the point shown with a red circle in Figure 3.17 (139E, 42N). The postseismic changes are modeled only with a single exponential function.

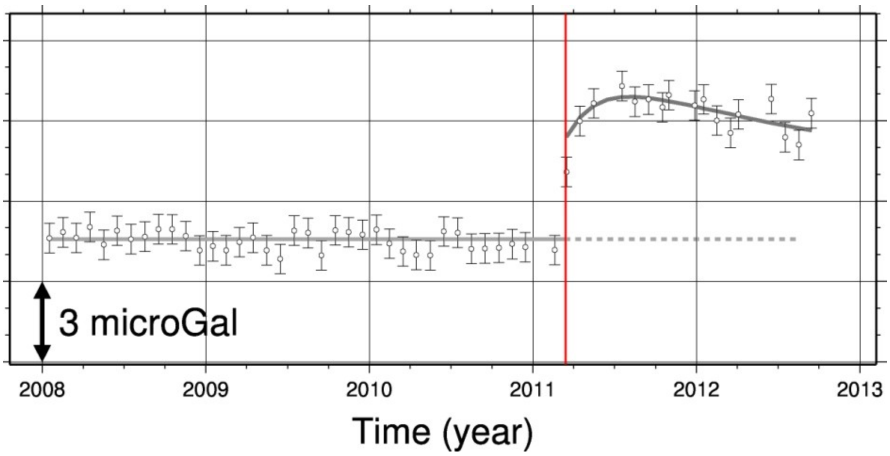

Figure 3.19 The time series of the northward gravity changes before and after the 2011 Tohoku-oki earthquake at the point shown with the blue circle in Figure 3.17 (139E, 36N). Two components of the postseismic gravity change are clearly seen although their statistical significance is not clear (because the middle panel of Figure 3.17 looks fairly noisy).

3.3 Contributions to geodynamics

This study suggests that the gravity is the unique method to separate two postseismic phenomena. Fault ruptures in earthquakes are observed with seismographs, and can be studied quantitatively in terms of surface displacements using GNSS networks. However, the two representative postseismic phenomena, i.e. afterslip and mantle relaxation, are difficult to separate with these conventional sensors. In this study, these two components of postseismic phenomena are suggested to emerge as the gravity changes with different polarities. This suggests the unique role of satellite measurement of time-variable gravity to separate these two processes.

It is important to understand postseismic phenomena in order to understand the physics behind earthquakes. It might be also important to investigate when and where earthquakes occur because the mechanisms of postseismic phenomena may also govern co- or preseismic processes. I would be happy if the present study could move the frontier of the knowledge farther ahead.

4. Summary

Satellite gravimetry is considered to be the third sensor to observe earthquakes after the networks of seismometers and GNSS receivers that observe seismic waves and static crustal deformation, respectively. The data from the GRACE satellites, which enable us to study time variable gravity fields of the earth, give us insight into phenomena involving mass movements at depth. They also let us know two-dimensional distribution of gravity changes associated with large earthquakes.

Three mega-thrust earthquakes, i.e. the 2004 Sumatra-Andaman earthquake, the 2010 Chile (Maule) earthquake, and the 2011 Tohoku-oki earthquake, occurred after the launch of the GRACE satellites in 2002. In this study, I studied the gravity changes associated with these earthquakes using the GRACE data. The main finding is that the postseismic gravity changes are composed of two distinct components, i.e. short- and long-term gravity changes. Coseismic gravity drops continue for a few months (short-term postseismic changes), and then gravity increases gradually over a year or longer (long-term postseismic changes). I tried F-test to check if the post-fit gravity residuals significantly decrease by assuming the two components, between the observation and the calculation. However, the decrease of the residual was not large enough to be significant from statistical point of view.

I also studied the changes in the north component of the gravity field because they are free from longitudinal stripes. Although clearer coseismic changes are observed in this component, their postseismic gravity changes did not suggest the existence of the two components so clearly as the vertical component.

The physical mechanisms of the short- and long-term postseismic gravity changes would be explained with afterslip and viscoelastic mantle relaxation, respectively, to some extent. However, they also have some problems. Afterslip has a problem of spatial pattern. The calculation of gravity changes caused by the afterslip gives the amplitude fairly consistent with the observations. However, its spatial distribution often does not match with the observed pattern sufficiently. Viscoelastic mantle relaxation has a problem in time constant. We could reproduce the spatial pattern consistent with the observed long-term postseismic changes of the 2004 Sumatra-Andaman earthquake by using the model by *Tanaka et al.* [2006; 2007]. However, we have to assume much lower viscosity of the upper mantle than those inferred by various observations. The long-term postseismic gravity changes of the 2010 Chile (Maule) and the 2011 Tohoku-oki earthquakes took only a few months to start increasing. Even if the upper mantle beneath the faults of the 2004 Sumatra-Andaman earthquakes has a fairly low viscosity, similar low viscosity upper mantle should also lie beneath the NE Japan and central Chile. I think it rather unrealistic that the viscosities of the rocks under the faults of all the three megathrust earthquakes are much lower than the global average. Then, other mechanisms may be needed to explain the long-term postseismic gravity changes.

The mechanisms of postseismic gravity changes are still ambiguous, and will need long discussion in the future. Nevertheless, the gravity observation is considered to be the important “third sensor” of earthquakes to investigate postseismic phenomena in an approach that the first (seismographs) and the second (GNSS and SAR) sensors cannot take.

5. Acknowledgements

I have many people whom I would like to give gratitude, and the first person must be Professor Kosuke Heki, my supervisor. I am sure that I could not do my study without him. He gives me warm eyes, many advices to break the walls that I get, many chances to take part in many scientific meetings and to discuss with scientists at other research institutions, jobs as a teaching assistant to solve my economic problems, and many other things which I got with a lot of gratitude. My gratitude to him is beyond description. I am proud that I am a student of him. I will also try to give him something for him and his study while I am at doctor course. Next, I would like to express my gratitude to Dr. Koji Matsuo, who was a senior student at our laboratory and is a postdoctoral researcher at Kyoto University. He also gave me many advices and told me how to use data especially when I was an undergraduate student and a master-course-first-grade student because we studied in the same room and with the same data. Those great helps always got my study much better. I would also like to say thanks to Prof. Yoshiyuki Tanaka at Tokyo University. He gave me the data of Figure 3.10 (right) and explained the theory I had to understand. This was a very big help for my study. I am also grateful to the teachers and students at the solid seminar in Hokkaido University. The teachers also gave me very suggestive advices and comments about my study when I made my presentation, which got my study advanced again and again. The students gave me a happy and exciting life in laboratory. And knowing what and how teachers and other students study in our seminar gets me excited very much. I am happy that I am going to be a doctor course student in this environment.

謝辞

本研究は，多くの方々の協力を賜って達成しました．ここにその謝辞を記します．

第一に，指導教官の日置教授に感謝を示したく思います．日置教授は私を見守ってくださり，時には私のつまずきを打破する助言をくださり，時には様々な学会や勉強会に参加して色々な研究者の方々と議論する機会を与えてくださり，また時にはティーチング・アシスタントの仕事を紹介してくださり，本当に様々な面で良くしていただきました．この感謝を示す適切な言葉を見つけようとしましたが，どうやらそれは私の能力を超えているようです．ただ，本当にありがとうございました．日置教授が指導教官で良かったと思っています．私は更に博士課程に進学いたしますが，そこでは私も教授の研究に貢献できるようなことをしたいと思います．今後ともよろしくお願いします．

次に，この研究室の先輩であり，現在は京都大学で研究者をしていらっしゃる松尾功二さんにお礼を申し上げます．特に私が修士 1 年だった昨年と，学部生だった一昨年は，同じ部屋で同じデータを使って研究していることもあり，多くの助言とご指導をいただきました．その助言とご指導が無ければ，私の研究がどうなっていたのか分からないほどです．厚くお礼申し上げます．ありがとうございました．

また，東京大学地震研究所の助教である田中愛幸さんにもお礼申し上げます．本研究の図 3.10（右）の結果は田中さんの計算結果を頂いたものであり，私が学ぶべき理論について説明していただくこともありました．観測データを解析するだけでなく，理論を学ぶことも非常に重要であり，その大きな助けをいただくことができました．

更に，私が所属している北海道大学の固体系ゼミの先生方，そして先輩方，同期，後輩の皆様に，ここでお礼を述べさせていただきます．先生方には，私の発表のときに大変有益なお言葉をいただき，それは私の研究を推し進める力になってくれました．また，研究室の生活が豊かなものになったのは，先輩方や同期，更には後輩の皆様のおかげです．ゼミで先生方や他の学生が一体どんな研究を，どのように行なっているのかを聞くと，とてもワクワクしました．この環境で博士課程に進めることを嬉しく思います．

皆様，本当にありがとうございました．これからもよろしくお願いします．

6. References

Banerjee, P., F. F. Pollitz, and R. Bu¨ rgmann, 2005: The size and duration of the Sumatra-Andaman earthquake from far-field static offsets, *Science, 308,* 1769 – 1772 doi: 10.1126/science.1113746

Chen, J. L., C. R. Wilson, B. D. Tapley, and S. Grand 2007: GRACE detects coseismic and postseismic deformation from the Sumatra-Andaman earthquake, *Geophys. Res. Lett., 34, L13302,* doi:10.1029/2007GL030356

Fei, H., M. Wiedenbeck, D. Yamazaki, T. Katsura, 2013: Small effect of water on upper-mantle rheology based on silicon self-diffusion coefficients, *Nature,* doi:10.1038/nature12193

Han, S.-C., and F. J. Simons (2008), Spatiospectral localization of global geopotential fields from the Gravity Recovery and Climate Experiment (GRACE) reveals the coseismic gravity change owing to the 2004 Sumatra-Andaman earthquake, *J. Geophys. Res., 113*, B01405, doi:10.1029/2007JB004927.

Han, S.C., Shum, C.K., Bevis, M., Ji, C., Kuo, C.Y., 2006: Crustal dilatation observed by GRACE after the 2004 Sumatra-Andaman earthquake, *Science, 313, 658-666,* doi:10.1126/science.1128661.

Heiskanen, W. and H. Moritz 1967, Physical Geodesy.

Heki K., and K. Matsuo, 2010: Coseismic gravity changes of the 2010 earthquake in Central Chile from satellite gravimetry, *Geophys. Res. Lett., 37,* L24306, doi:10.1029/2010GL045335.

Imanishi, Y., T. Sato, T. Higashi, W. Sun, and S. Okubo, 2004: A network of superconducting gravimeters detects submicrogal coseismic gravity changes, *Science, 306, 476-478.*

Kaula 1966, Theory of satellite geodesy: Applications of satellites to geodesy

Matsuo, K., and K. Heki, 2011: Coseismic gravity changes of the 2011 Tohoku-Oki Earthquake from satellite gravimetry, *Geophys. Res. Lett., 38,* L00G12, doi:10.1029/2011GL049018, 2011.

Ogawa, R., and K. Heki 2007: Slow postseismic recovery of geoid depression formed by the 2004 Sumatra - Andaman earthquake by mantle water diffusion, *Geophys. Res. Lett., 34*, L06313, doi:10.1029/2007GL029340.

Ozawa, S., T. Nishimura, H. Suito, T. Kobayashi, M. Tobita, and T. Imakiire, 2011: Coseismic and postseismic slip of the 2011 magnitude-9 Tohoku-Oki earthquake, *Nature,* doi:10.1038/nature10227.

Panet, I. et al., 2007. Coseismic and post-seismic signatures of the Sumatra 2004 December and 2005 March earthquakes in GRACE satellite gravity, *Geophys. J. Int., 171*, 177–190.

Rodell, M., and Houser, P. R., Jambor, U., Gottschalck, J., Mitchell, K., Meng, C.J., Arsenault, K., Cosgrove, B., Radakovich, J., Bosilovich, M., Entin, J.K., Walker, J.P., Lohmann, D., Toll, D., 2004: The Global Land Data Assimilation System. *Bull. Am. Meteorol. Soc. 85, 381-394.*

Sun, W., S. Okubo, G. Fu, and A. Araya, 2009: General formulations of global and co-seismic deformations caused by an arbitrary dislocation in a spherically symmetric earth model － applicable to deformed earth surface and space-fixed point, *Geophys. J. Int., 177, 817-833.*

Swenson, S., and J. Wahr, 2006: Post-processing removal of correlated errors in GRACE data, *Geophys. Res. Lett., 33,* L08402, doi:10.1029/2005GL025285.

Tanaka, Y., Okuno, J. and Okubo, S. (2006), A new method for the computation of global viscoelastic post-seismic deformation in a realistic earth model (I)—vertical displacement and gravity variation. *Geophys. J. Int.*, 164: 273–289. doi: 10.1111/j.1365-246X.2005.02821.x

Tanaka, Y., Okuno, J. and Okubo, S. 2007: A new method for the computation of global viscoelastic post-seismic deformation in a realistic earth model (II)-horizontal displacement. *Geophys. J. Int., 170:* 1031–1052. doi: 10.1111/j.1365-246X.2007.03486.x

Wahr, J., M. Molenaar, and F. Bryan, 1998: Time variability of the Earth's gravity field: Hydrological and oceanic effects and their possible detection using GRACE, *J. Geophys. Res., 103*, 30205-30229, doi:10.1029/98JB02844.

Wang, L., C.K. Shum, F. J. Simons, B. Tapley, and C. Dai 2012: Coseismic and postseismic deformation of the 2011 Tohoku-Oki eaerthquake constrained by GRACE gravimetry, *Geophys. Res. Lett., 39*, L07301, doi:10.1029/2012GL051104.

Zhang, Z., B. F. Chao, Y. Lu, and H. T. Hsu, 2009: An effective filtering for GRACE time-variable gravity: Fan filter, *Geophys. Res. Lett., 36*, L17311, doi: 10.1029/2009GL039459